University of Tartu

Faculty of Science and Technology

Institute of Ecology and Earth Sciences

Department of Geology

Master Thesis in Geology (30 ECTs)

In situ detrital zircon U-Pb age dating of Lastoursville Sub-Basin carbonate-black shale deposits in Francevillian Basin, Gabon

Carmel Kuusk

Supervisor: Kalle Kirsimäe

Tartu 2024

In situ detrital zircon U-Pb age dating of Lastoursville Sub-Basin carbonate-black shale deposits in Francevillian Basin, Gabon

The aim of this master thesis was, first, to test the applicability of the *in situ* zircon U-Pb dating technique on small zircon grains from carbonate and black-shale rocks and, second, to refine the maximum depositional ages of the Paleoproterozoic sediments in the FB/FC formations of the Francevillian Basin in Gabon.

Studied material was sampled in the carbonate-black-shale succession opened in LST12 drill core Lastoursville Sub-Basin of the Francevillian Basin. For detrital zircon dating drill core samples were scanned with a hand-held X-ray fluorescence spectrometer for the highest Zr content, and samples with zircon content over 400 ppm were chosen for further analysis. Three samples had zircon grains suitable for U-Pb dating using laser-ablation inductively coupled plasma mass spectrometry. The zircon grains yielded Pb-Pb ages mostly around 2860 Ma and did not show any systematic variation with respect to the zircon grain size. In one sample from the upper part of the studied succession, there was an indication of a population with Pb-Pb ages at ca 2200 Ma, which defines the maximum age of the sediments. Numerous zircon grains had microscopic galena (PbS) inclusions in them, and such grains were not suitable for U-Pb dating. The galena inclusions are a result of hydrothermal alterations; however, the timing and wider implications of such hydrothermal event(s) on the preservation state of the Francevillian sediments remain debatable.

Keywords: U-Pb dating, LA-ICP-MS, detrital zircons

CERCS: P420 Petrology, mineralogy, geochemistry

Detriitsete tsirkoonide *in situ* dateerimine U-Pb meetodil Gaboni Franceville'i settebasseini Lastoursville'i alambasseini karbonaatsetest kihtidest ja mustadest kiltadest

Selle magistritöö eesmärgid olid esiteks selgitada *in situ* U-Pb meetodi kasutamisvõimalused väikesemõõduliste (<100 µm) detriitsete tsirkoonide dateerimiseks karbonaatsetes ja musta kilda setetes ja teiseks täpsustada Paleoproterosoilise Franceville'i settebasseini (Gabon) FB-FC kihtide maksimaalset settimisvanust.

Uuritud materjal pärines karbonaatide-mustade kiltade läbilõikest, mida avab LST12 puursüdamik Franceville'i settebasseini Lastoursville'i alambasseinis. Detriitsete tsirkoonide analüüsimiseks skaneeriti puursüdamiku proovid esmalt käsi-röntgenfluorestsents spektromeetriga, et leida kõrgeima tsirkoonisisaldusega intervallid. Proovid, kus tsirkoonisisaldus oli üle 400 ppm valiti edasisteks analüüsideks. Kolm proovi sisaldasid tsirkooniterasid, mis sobisid U-Pb dateerimiseks laser-ablatsiooni induktiivsidestatud plasma massi-spektromeetria meetodil. Tsirkooniterade Pb-Pb vanused olid valdavalt ca. 2860 Ma ja tsirkoonide vanustes ei olnud süstemaatilist varieeruvust seoses terasuurusega. Ühes uuritud läbilõike ülemise osa proovis leiti viiteid terade populatsioonile, mille Pb-Pb vanus on 2200 Ma, mis määrab setete maksimaalse vanuse. Paljud proovides leitud tsirkooniterad sisaldasid galeniidi (PbS) suletisi ja seetõttu ei sobinud U-Pb dateerimiseks. Galeniidi suletised on arvatavasti tekkinud hüdrotermaalsete protsesside tulemusena, kuid nende sündmuste vanus ja laiem mõju Franceville'i settebasseini setete säilivusele ei ole veel selge.

Märksõnad: U-Pb dateerimine, LA-ICP-MS, detriitsed tsirkoonid

CERCS: P420 Petroloogia, mineraloogia, geokeemia

Content

Introduction

The Francevillian Basin of Gabon contains a thick Paleoproterozoic volcanic-sedimentary succession (Gauthier-Lafaye & Weber, 1989; Ossa Ossa et al., 2013; Weber, 1968). It has been only mildly deformed into open folds and cut by high-angle faults (Gauthier-Lafaye & Weber, 1989) and has retained late-diagenetic to lower-greenschist metamorphic grade (<300 °C; Ossa Ossa et al., 2013) while most of the Paleoproterozoic sedimentary successions are overprinted by metamorphism ranging from upper greenschist (300–450 °C) to amphibolite-granulite grade (>500 °C and higher). This makes Francevillian Basin one of the best-preserved successions of its age in the world (Gauthier-Lafaye & Weber, 1989, 2003).

Sedimentary successions of the Francevillian Basin record important hallmarks in the evolution of the Earth's surface environments – the largest-magnitude perturbation of the carbon cycle – the Lomagundi-Jatuli Event (LJE), that occurred between 2.2-2.06 Ga (Karhu & Holland, 1996) in parallel to the build-up of a sizable sulfate marine reservoir (Blättler et al., 2018); the ca. 2 Ga Shunga Event – a large-scale accumulation of organic-rich sediments (Melezhik et al., 2012); and the appearance of the first phosphatic sediments (Lepland et al., 2013). Additionally, the Francevillian Basin sedimentary succession is known for natural fossil fission reactors, the earliest putative macrofossils, and large U and Mn ore resources (El Albani et al., 2010; Gauthier-Lafaye & Weber, 1989; Ossa et al., 2018).

All these were triggered by the shift from anoxic to oxic surface environments at Archean to Proterozoic transition (Holland, 2006; Lyons et al., 2014). The rise of oxygen levels in atmosphere – the Great Oxidation Event (GOE) - is dated between 2426 to 2460 Ma (Farquhar et al., 2000; Gumsley et al., 2017; Luo et al., 2016), but timing and tempos of GOE and particularly the nature and duration of the LJE are still largely debated (Gumsley et al., 2017; Hodgskiss et al., 2023; Martin et al., 2013; Poulton et al., 2021; Prave et al., 2022)

However, depositional age constraints for the Francevillian Basin are few. Zircons from a granite in the N'Goutou Complex yield a Pb-Pb date of 2191 ± 13 Ma (Sawaki et al., 2017) but the Complex's relationship with FA–FC formations in different sub-basins is unclear. A syn-depositional tuff in FD formation in the Franceville Sub-Basin has been dated at 2083 ± 6 Ma (Horie et al., 2005) but has been later questioned (Weber et al., 2016). The most recent are the Re-Os ages of 2107.3 ± 5.1 Ma and 2085 ± 13.7 Ma (Eyster et al., 2022) from organic-rich units of FB-FC formations in the Lastoursville Sub-Basin.

Detrital zircon U–Pb geochronology is a fundamental tool in studying clastic sedimentary systems, as zircons are resilient against both physical and chemical alterations, and reliable in geochronometry (Fedo et al., 2003; Gehrels, 2011). This technique is important for understanding source-to-sink relationships, maximum depositional ages, stratigraphy, and paleogeographic reconstructions (Cawood & Nemchin, 2000; Gehrels, 2014; Nelson, 2001).

Detrital zircon U-Pb ages of the sandstone lithologies in Francevillian succession have been studied before by Mathieu et al. (2001) and Ossa-Ossa et al. (2020) who have shown that age distribution of the detrital zircons is narrowly between ca. 3.10 to 2.60 Ga with a dominant population between ca. 2.90 and 2.80 Ga. This points to weathering and erosion of Archean rocks of the north and south Gabon massifs in Congo craton as the source of siliciclastic sediments to the Francevillian basin (Ossa Ossa et al., 2020) but also raises a question why there are no younger detrital zircons in the Francevillian sediments although Eburnean domains (2100-1980 Ma) and pre-Eburnean gneiss-migmatite complexes (2500-2120 Ma) occur in West Gabonian block (Ossa Ossa et al., 2020).

The aims of this study were, first, to test the applicability of the *in situ* zircon U-Pb dating technique on small (<100 μm) grains from carbonate and black-shale rocks that are not typically targeted for detrital zircons investigations, and second, to refine the maximum depositional ages of sediments in the LST12 drill core recording the purported decline from the positive carbonate carbon isotopic values characteristic to LJE to normal isotopic values.

1. Francevillian Basin

1.1. Location and general geology

Francevillian Basin is a geological structure in southeast of Gabon on the western margin of Congo craton (Figure 1). It spreads over 42 000 km^2 and the maximum thickness of the sedimentary infill in graben-like structures can be up to 2 km. The crystalline granitoid-greenstone basement is of Archean age, and it is unconformably covered with volcanoclastic-sedimentary group of the Paleoproterozoic age. Sediments in the eastern part of the basin are practically unmetamorphosed reaching regionally maximum up to lower-greenschist facies as evidenced by well-preserved clay minerals (Ossa Ossa et al., 2013) and lack of minerals indicative of higher metamorphic grades. Clay minerals in FA formation of the Franceville Sub-Basin reflect fluidal activity with temperatures mostly of 240 ± 30 °C and synchronous with quartz cementation, oil migration, and dissolution-precipitation of U-bearing phases at 2040–2010 Ma (Ossa Ossa et al., 2014).

Higher greenschist metamorphosis and folding have only taken place in the western part of sedimentary succession due to tectonic influences of Eburnean Orogeny (Thiéblemont et al., 2009). This means it is one of the best preserved late-diagenetic sedimentary successions of its age and, being deposited during the first oxidation of Earth's atmosphere, it proves to be a unique research area for geologists (Gauthier-Lafaye & Weber, 1989).

Francevillian Basin is divided into four sub-basins: Booué, Lastoursville, Okondja and Franceville (Ossa Ossa et al., 2018). The Franceville Sub-Basin is best known because of its mineralized uranium and manganese deposits, which is the reason for thorough geological information being collected from the basin. In addition to that, the basin hosts natural nuclear fission reaction zones in the uranium deposits (Gauthier-Lafaye & Weber, 1989).

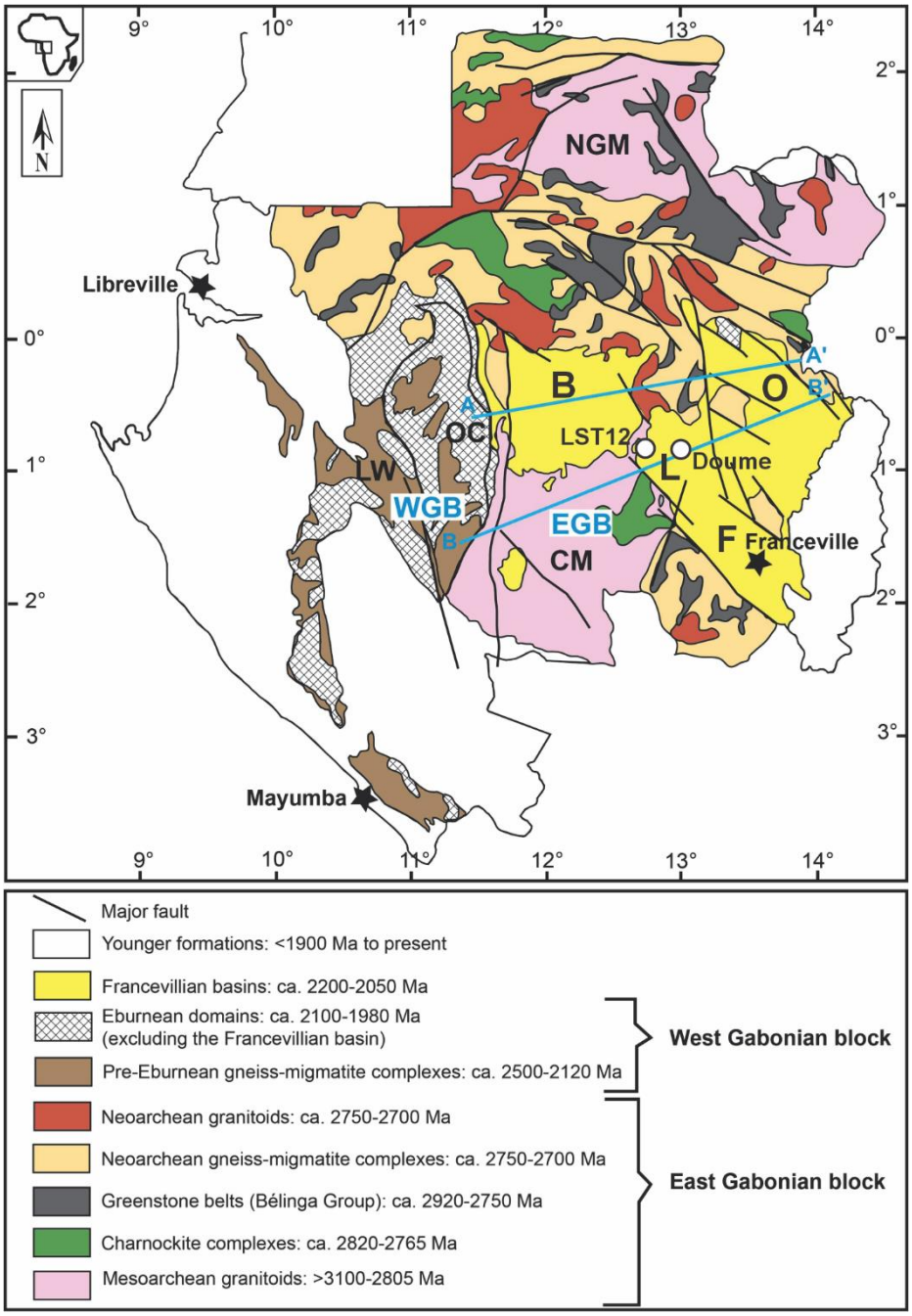

Figure 1. Geological map of Gabon with the location of the LST12 and Doumé drill cores. A-A' and B-B' lines are WSW-ENE and SW-NE cross-sections shown in Figure 10. F – Franceville Sub-Basin; L – Lastoursville Sub-Basin; B – Booué Sub-Basin; O – Okondja Sub-Basin; WGB - West Gabonian Block; EGB - East Gabonian Block; NGM - North Gabon Massif; CM - Chaillu Massif; LW - Lambaréné-Waka; OC - Ogooué Complex (modified from Thiéblemont et al., 2009; and Ossa Ossa et al., 2020).

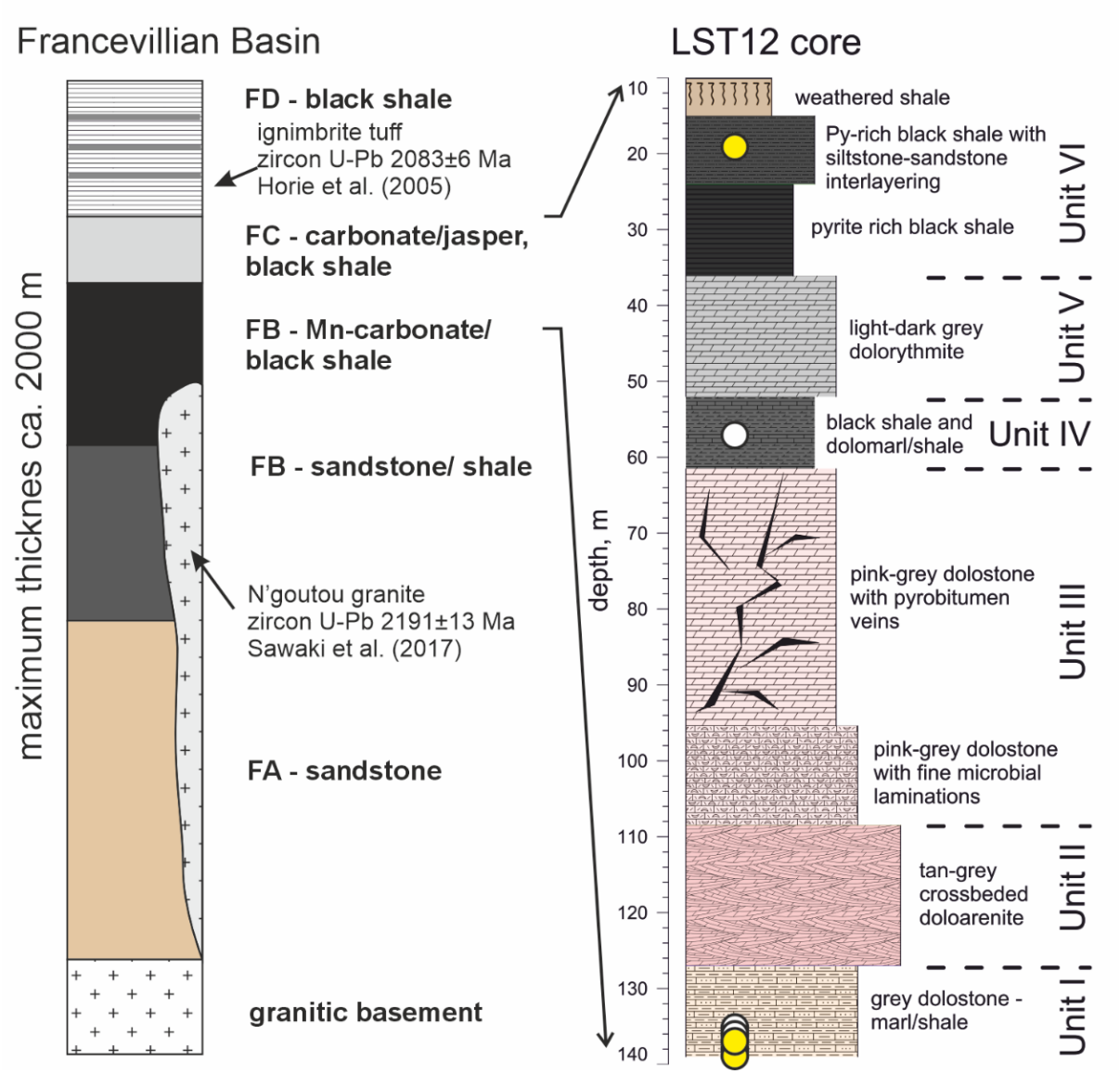

Figure 2. General stratigraphy and lithology of the Franceville Basin and the LST12 drill core succession (modified after Mayika et al., 2020 and Juhkama, 2020). Circles on LST12 profile mark the location of studied samples. Yellow fill indicates samples where detrital zircons were dated.

The sedimentary succession is divided into five lithological units from FA to FE, FA being stratigraphically the lowest and FE the uppermost unit (Figure 2). The Francevillian A (FA) unit consists of deltaic and fluviatile deposits. The lowest part of the unit contains coarse, poorly sorted sandstones with red U-bearing conglomerates in thin layers that are covered with 2 to 7 coarsening-upward sequences from marine shales to coarse-grained conglomeratic sands. These sequences contain uranium mineralization in southeastern part of the basin. They are covered with a unit of tidal deposits of fine-grained sandstones and shales. This in turn is overlain by fluviatile sediments with uranium mineralization. The upper part of unit FA is represented by deltaic deposits. The quartz grains in all sandstones in this unit are well-

rounded, suggesting many cycles of erosion and sedimentation. (Gauthier-Lafaye & Weber, 1989, 2003)

The Francevillian B (FB) formation is divided into two subunits: FB1 and FB2. The lower part of unit FB1 is mainly composed of organic-rich black shales and turbiditic sandstones. The upper part of the unit is represented by iron and manganese rich carbonates. Tectonic activity has been proposed during FB1 sedimentation to explain great thickness variations in the formation within the basin (Gauthier-Lafaye & Weber, 1989). The FB2 unit is made of massive sandstones called Poubara sandstones with occasional black shales interlayers. Poubara sandstones are interpreted as turbiditic, deltaic or storm-wave deposits. K-bentonite beds are also found there. The sandstones are capped with organic rich black shales and siltstones. In Booué Sub-Basin and on the highlands separating Franceville Sub-Basin from Okondja Sub-Basin the FB pelitic sandstones and shales are absent. In some areas even FA deposits can be missing, so FC formation lies directly on Archean basement. In the Okondja Sub-Basin the FA and FB formations are cut by intruding igneous pluton called N'Goutou complex. (Bankole et al., 2018; Weber et al., 2016)

The Francevillian C (FC) formation consists of evaporitic dolomites and stromatolitic cherts that are interlayered with black shales. In Franceville and Okondja Sub-Basins the uppermost layer of the FC unit also contains pyroclastic sediments. The Francevillian D (FD) unit begins with organic-rich black shales interlayered with pyroclastic beds. The tuff beds were produced by explosive volcano eruptions of andesitic to rhyolitic magmas. The composition of tuffs is chemically different from magmas that formed N'Goutou intrusions, suggesting that tectonic situation must have changed between formation of FB and FD units. The sedimentary succession of the Francevillian Basin is completed by the Francevillian E (FE) formation that contains two large sequences of sandstones where rare ignimbrite pebbles occur as well. (Weber et al., 2016)

All known uranium ore deposits are located in the FA formation in Franceville Sub-Basin. They derive from Th-U-rich conglomerates in the base of the formation (Mathieu et al., 2001). The uranium ores formed roughly 2.0 Ga ago when oxidized fluids mobilized uranium from the deposits. Accumulation happened as the uranium-rich fluid was transported to more reduced environments, such as petroleum reservoirs, and uranium precipitated, forming high-grade ores where natural fission reactions can be sustained in the presence of water or graphite. Deposits are related to geological traps for both uranium and petroleum, capped with

impermeable black shales of FB formation. Natural fission reaction zones are surrounded by clays that are a result of hydrothermal alteration induced by the thermal emission of the reactors. (Gauthier-Lafaye & Weber, 1989, 2003)

The Archean basement of Francevillian Basin consists of metamorphosed terrains intruded by plutons that have been dated by U-Pb ages between 2998 ± 25 Ma to 2922 ± 24 Ma (Mouélé et al., 2014). N'Goutou igneous complex intruding the FA and FB formations in Okondja Sub-Basin has been dated by Moussavou & Minko (2006) and Sawaki et al. (2017) by zircon grains separated from the granites and syenites yielding U-Pb ages of 2027 ± 55 Ma and 2191 ± 13 Ma, respectively. Therefore, formations FA and FB cannot be any younger.

Clay fractions of manganese-rich carbonates from FB unit were dated by Bros et al. (1992) and Stille et al. (1993) using Sm-Nd method yielding ages of 2099 ± 115 Ma and 2036 ± 70 Ma. (Weber et al., 2016)

The ignimbrites in FD formation were dated by zircon U-Pb method at 2083 ± 6 Ma by Horie et al. (2005). However, Weber et al. (2016) expressed doubts about these ages because the age was received from a mix of two populations of zircons with different ages. One population yielded ages from 2136 to 2068 Ma and second one from 2042 to 2003 Ma. Weber et al. (2016) suggested that the older set was most possibly obtained from the basement whereas younger ages may reflect the true sedimentation age of tuff beds.

The dolerite dykes intersecting with the succession in Franceville Sub-Basin as a result of the latest tectonic event there have been dated by K-Ar method to 970 ± 30 Ma (Bonhomme et al., 1982 *cit.* Gauthier-Lafaye & Weber, 2003).

The most recent age constraints are for Lastoursville Sub-Basin FB and FC formations by Eyster et al. (2022). Re-Os dating yielded ages of 2107.3 ± 5.1 Ma and 2085 ± 13.7 Ma, respectively.

In addition to the radioactive decay methods the Francevillian succession has been correlated to the Paleoproterozoic sedimentary basins worldwide using carbon isotope excursions that have often been used to correlate different sedimentary strata of same age from all over the world. The Paleoproterozoic after the Great Oxidation Event is marked by the longest-lived and highest amplitude carbon isotopic excursion – the Lomagundi-Jaguli Event (LJE) that is also recorded in carbonates of the Francevillian Basin tying the sediments to the LJE (Préat et al., 2011; Weber & Gauthier-Lafaye, 2013). However, Mayika et al. (2020) have shown that

carbon isotope excursion in Lastoursville Sub-Basin is facies related and the use of this event as a global stratigraphic correlation tool calls for caution.

2. Detrital zircon dating

Detrital zircon analysis is a significant methodological approach in geology, facilitating the reconstruction of the geological history of sedimentary basins and their adjacent source regions through the examination of zircon provenance. Over the past decades, detrital zircon geochronology has undergone rapid advancement, transitioning from a technique with perceived limitations to an indispensable tool for investigating sedimentary units and their associated source regions. This transformative progression, colloquially termed the "DZ revolution," can be largely attributed to the widespread adoption of laser-ablation inductively coupled plasma mass-spectrometers (LA-ICP-MS) since the late 1990s. This technology enables the efficient determination of U-Pb ages on individual zircon crystals. (Gehrels, 2011)

Presently, detrital zircon geochronology serves as the cornerstone for four principal applications (Andersen, 2005; Fedo et al., 2003; Gehrels, 2011):

a) Provenance studies: This involves the comparison of ages of detrital minerals with those of potential source terranes to discern the ultimate origins of sediment.
b) Source terrane characterization: Once provenance is established, this application entails determining the ages and characteristics of rocks within the identified source terranes.
c) Sedimentary unit correlation: By comparing ages of detrital minerals, this application aims to evaluate potential linkages between different sedimentary units.
d) Maximum depositional age determination: This method utilizes the youngest age component in a clastic unit to infer the earliest possible age of deposition.

Ideally, the analyzed sample would comprehensively represent geological history, encompassing evidence of all possible provenances and their interrelationships. However, natural complexity and artificial bias hinder achieving such completeness.

Biases in detrital zircon age populations can arise from both natural geological and laboratory factors (Barham et al., 2021; Chew et al., 2020; Dröllner et al., 2021; Fedo et al., 2003; Sláma & Košler, 2012).

Geological biases such as variable source rock characteristics and sedimentary processes are inherent to detrital zircon investigations but can be mitigated through strategic sampling (Spencer et al., 2018). For example, zircon is typically absent in ultramafic/mafic igneous rocks, so their contribution to sedimentary deposits can be underestimated. Additionally,

zircons are not fully resistant to weathering, therefore older, higher-U grains may be eliminated at some point. (Fedo et al., 2003)

Laboratory biases, including sampling and processing techniques, may compromise the representativeness of detrital zircon populations (Dröllner et al., 2021; Hietpas et al., 2011; Malusà et al., 2016; Moecher & Samson, 2006; Sircombe & Stern, 2002). These biases can affect interpretations of provenance and maximum depositional ages, necessitating careful consideration of relative age mode significances (Barbeau et al., 2009; Sharman & Malkowski, 2020; Vermeesch, 2021). Sample preparation bias begins with sample selection which is influenced by rock type and depositional setting. Later, physical sample preparation, such as crushing and milling, introduces other biases, especially size grading. The entire detritus set might not be represented by zircons, as units with low zircon abundance would be under-represented in samples. (Fedo et al., 2003) Moreover, analyzing grains >100 μm biases interpretations toward coarse-grained granitoids (Gehrels, 2000 *cit.* Fedo et al., 2003).

Confidently determining accurate maximum depositional ages, especially in subsurface basin sequences, remains challenging due to sample recovery limitations and stratigraphic complexities (Hilbert-Wolf et al., 2017; Macdonald et al., 2013). Thus, developing methodologies to ensure the recovery of representative zircon age populations has been pointed out as crucial for robust determinations of sediment provenance and depositional age (Bowring et al., 2006; Gehrels, 2011).

Recently Zutterkirch et al. (2021) proposed a methodology for evaluating whether the dated zircon grain sizes accurately represent the overall grain sizes preserved within a sample, utilizing *in situ* zircon dating in thin sections. This approach demonstrates potential in detecting and quantifying the mineral composition of zircon-bearing rock fragments within a sedimentary rock, enabling comparison with possible source region rock compositions. Additionally, Zutterkirch et al. (2021) suggest that thin tuff layers, crucial for determining absolute depositional ages, can be more readily identified using this method. Moreover, they showed that the determination of maximum depositional ages of *in situ* measured grains is more robust compared to grain ages measured on conventional mounts.

3. Material and methods

Material for this study was obtained from the Francevillian basin, Lastoursville Sub-Basin, Gabon that opens FB and FC formations (Figure 2). The previous geochemical analyses of 139 m long LST12 core were made at ca 2 m interval (Juhkama, 2020; Mayika et al., 2020). Based on these results the drill core intervals at depths 18.9-60 m, 80-90 m, and 110-139 m were selected for detailed scanning with hand-held X-ray fluorescence (XRF) spectrometer of all available samples that were taken from the core at a sampling interval from ca. 0.5 to 1 m. To ensure enough zircon grains for dating, samples with zircon content over 400 ppm were chosen for further studies. According to Zr screening slabs from depths of 18.9 m, 57.5 m, 136.0 m, 136.8 m, 137.0 m, 138.0 m, and 138.7 m were selected, cut, and polished for further analysis.

First, samples were studied with scanning electron microscope (SEM) for zircon grains identification and mapping. Sufficient number of zircon grains suitable for dating were located in samples from depths of 138.7 m, 137.0 m, and 18.9 m. Zircons were chosen for dating randomly all over the sample surface, if grains were large enough to host a laser spot of 20 µm. Sample from 57.5 m did not have any visible zircon grains in it. Other prepared slabs contained zircons with Pb inclusions in them. Such grains are not useful for U-Pb dating as there would be excess lead concentrations.

SEM imaging of polished slabs was done using a ZEISS EVO MA15 SEM. First screening was done in variable pressure (VP) mode and chemical characterization by elemental mapping of the samples was carried out with Oxford AZTEC-MAX energy-dispersive spectroscopy detector (EDS) attached to SEM. To identify the accurate chemical composition of Pb inclusions in zircons, wave-length dispersive (WDS) detector Wave700 on the same SEM was used for analyses performed in high vacuum (HV) mode. To reduce the charging effects of these non-conductive rock samples, a thin coating of ca. 5-10 nm thick carbon was used. Using SEM imaging coordinated maps for each sample suitable for dating with locations of identified zircon grains were created and loaded to inductively coupled plasma mass-spectrometry (ICP-MS) control software prior analysis.

The U and Pb isotopic composition of the samples was measured in four sessions using Agilent 8800 inductively coupled plasma mass-spectrometer coupled to a Cetac LSX213 G2+ laser and HelExII ablation cell. Measurements were carried out using 20 µm spot size, 4 Hz repetition rate and fluence of 5.76 J/cm^2. Ablations lasted for 50 s and were preceded by 20 s of

background measurements. Masses ^{178}Hf, ^{202}Hg, ^{204}Pb, ^{206}Pb, ^{207}Pb, ^{208}Pb, ^{232}Th and ^{238}U were measured. International zircon standard 91500 (age 1062.4 ± 0.4 Ma, Wiedenbeck et al., 1995) and *in-house* standard Scottish Small (age 2464 ± 12 Ma; Faithfull et al., 2018) described in Ausmeel, (2020) were used for calibration and data quality control after every 10 to 15 unknowns. Data reduction was made in the program Iolite 4.8.2 and MS Excel Isoplot 4.15 was used to analyse concordance of the results. The zircon standard 91500 and Scottish Small yielded average ages 1063.3 ± 3.0 Ma and 2499.78 ± 64 Ma during the analytical sessions.

4. Results

Geochemical analyses

Results of the both ICP-MS and hand-held XRF analyses of selected samples from LST12 drill core are shown in Figure 3 and Table 1. According to XRF analyses, three intervals at ca. 18–20 m, 50–60 m, and 136-139 m had zirconia content over 200 ppm. These intervals correspond to the interlayered pyrite rich shale-siltstone-sandstones of Unit VI; alternating (black)shale and dolomarl in Unit IV and dolomarls-shales of Unit I, respectively (Figure 3). The units composed of dominantly carbonate rocks had very low Zr content and therefore had low potential for finding zircons for U-Pb dating. In most Zr-rich intervals, samples with Zr content >400 ppm were chosen for further studies.

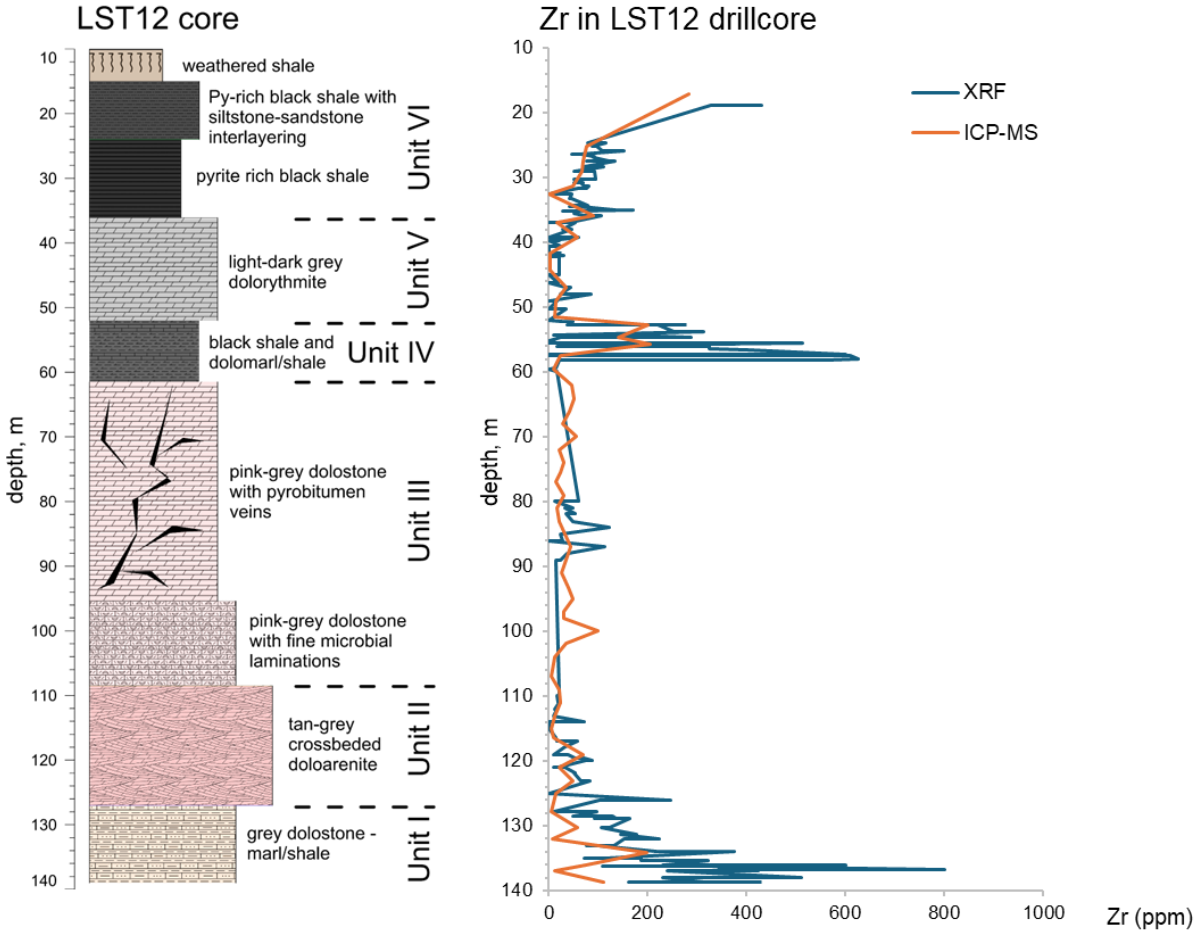

Figure 3. Zircon content in LST12 drill core samples based on ICP-MS and XRF analyses. Drill core lithology and ICP-MS data from Juhkama, 2020.

Table 1. Zr content measurements from ICP-MS (Juhkama, 2020) and XRF in LST12 drill core samples.

ICP-MS		XRF							
Depth (m)	Zr (ppm)	Depth (m)	Zr (ppm)	Depth (m)	Zr (ppm)	Depth (m)	Zr (ppm)	Depth (m)	Zr (ppm)
17.2	282.2	18.9	430.0	39.2	0.0	56.1	22.0	121	19.0
25.145	76.9	18.9	327.0	39.2	61.0	56.1	24.0	121	10.0
27.415	69.3	24.575	79.0	39.75	0.0	56.1	325.0	121	33.0
29	67.6	24.575	115.0	39.75	18.0	56.48	324.0	121.86	53.0
31.37	47.8	25.145	87.0	39.75	0.0	56.52	403.0	121.86	51.0
32.525	1.3	25.145	96.0	39.75	0.0	57.25	600.0	123	65.0
34.225	49.3	25.9	108.0	39.75	0.0	57.28	556.0	123	84.0
35.875	89.4	25.9	152.0	40.6	26.0	57.28	0.0	125	0.0
37	16.9	26.465	57.0	40.6	0.0	57.5	24.0	126	247.0
39.2	58.1	26.465	47.0	41.68	0.0	57.535	0.0	126.07	130.0
41.68	2.0	26.465	68.0	41.68	0.0	57.535	610.0	126.07	101.0
44.35	3.7	26.7	93.0	41.68	21.0	58.07	626.0	127.8	10.0
47	34.5	26.7	87.0	41.68	0.0	58.1	559.0	127.8	97.0
49.05	13.5	26.91	93.0	42	0.0	58.1	22.0	128.51	48.0
51.5	10.7	26.91	92.0	42	0.0	59.46	14.0	128.51	129.0
52.75	199.3	27.415	123.0	42	0.0	59.46	12.0	128.8	136.0
54.585	140.1	27.415	76.0	42	31.0	59.515	0.0	128.8	92.0
55.695	205.5	27.415	133.0	42.2	0.0	60	17.0	128.8	163.0
57.535	22.5	28.4	70.0	42.2	22.0	80	59.0	130.3	123.0
59.515	9.1	28.4	110.0	45	22.0	80	11.0	130.3	123.0
62	45.7	29	51.0	45	0.0	81	49.0	130.3	106.0
64.2	50.9	29	50.0	46.155	19.0	81	32.0	131.4	177.0
66	41.8	29	67.0	46.155	0.0	81.76	53.0	131.4	146.0
68	27.2	29.12	81.0	47	34.0	81.76	35.0	132	224.0
70	55.3	29.12	92.0	47	45.0	81.815	35.0	132	202.0
72	21.5	30.32	94.0	48	24.0	83	49.0	132.09	156.0
73.95	30.3	30.32	52.0	48	85.0	84	123.0	132.09	152.0
75.5	23.9	30.77	58.0	49.05	0.0	85	24.0	133	131.0
77	14.9	30.77	65.0	49.05	17.0	86	28.0	133	76.0
79	30.1	30.77	50.0	50.2	0.0	86	0.0	133	103.0
81	15.6	30.77	69.0	50.2	34.0	86.85	114.0	134	218.0
83	21.2	30.77	65.0	51.95	0.0	88	36.0	134	375.0
85	31.9	31.37	72.0	51.95	0.0	89	24.0	135	112.0
86.925	43.4	31.37	80.0	52.2	27.0	89	13.0	135	72.0
91	26.5	31.765	77.0	52.2	49.0	110	21.0	135	186.0
93.17	38.6	31.765	58.0	52.75	37.0	110	16.0	135.4	187.0
95	48.1	32.525	0.0	52.75	275.0	111	19.0	135.4	294.0
96.95	30.7	32.525	46.0	52.75	199.0	111	22.0	135.4	323.0
97.95	30.6	33.175	42.0	52.75	222.0	112.1	12.0	136	231.0
99.985	98.2	33.175	46.0	53.8	253.0	112.1	16.0	136	600.0
101.85	35.2	34.225	79.0	53.8	313.0	113	9.0	136.14	108.0
104	11.0	34.225	43.0	54.25	10.0	113	10.0	136.14	332.0
106.9	5.5	34.525	80.0	54.29	23.0	114	71.0	136.8	800.0
109	20.3	34.525	65.0	54.29	29.0	114	0.0	136.8	527.0
111	22.3	34.525	42.0	54.56	226.0	114	0.0	136.8	343.0
113	11.5	34.525	65.0	54.585	287.0	115	0.0	137	423.0
115	5.9	35.03	136.0	54.585	24.0	116.44	14.0	137	239.0
116.49	8.4	35.03	170.0	55.15	0.0	116.44	13.0	138	511.0
119	69.9	35.1	28.0	55.185	0.0	117	16.0	138	230.0
121	20.7	35.1	54.0	55.185	0.0	117	43.0	138.7	318.0
123	49.0	35.475	56.0	55.5	16.0	117	58.0	138.7	426.0
125	15.2	35.475	52.0	55.5	0.0	117.8	32.0	138.7	161.0
127.8	4.7	35.875	74.0	55.5	28.0	117.8	33.0		
130.3	57.5	35.875	107.0	55.5	513.0	119	9.0		
132	7.0	37	41.0	55.66	261.0	119	39.0		
134.045	197.6	37	0.0	55.695	373.0	119.5	53.0		
136	74.1	37	54.0	55.695	31.0	119.5	72.0		
136.85	12.4	38.035	27.0	56.1	23.0	120	88.0		
138.7	110.3	38.035	46.0	56.1	17.0	120	73.0		

SEM imaging

The identification of zircon grains was performed using SEM imaging. Because of the high average atomic weight of zircon, the zircon grains show up on back-scattered electron detector imaging as bright grains, so this was used to locate the grains (Figures 4a; 5). Zircon identification was confirmed with X-ray energy-dispersive spectroscopy (EDS) detector attached to SEM. Most of the identified zircon grains had growth zones recognisable in SEM images (Figures 4a; 5a, b, f). The size of zircon grains varied around 30 to 50 µm by longer axis (Figure 5). Also, most zircons had easily distinguishable zircon crystal shape, although many looked as if they had been broken recently with only half of the core and surrounding growth zones showing on images (Figures 4a; 5d). There were many grains that had bright inclusions. The EDS analyses of the inclusions revealed presence of Pb (Figure 4b). However, as the spectral resolution of the EDS does not allow separation of Zr, Pb and S peaks, then it was not possible to determine if the inclusions are composed of native Pb or galena (PbS). The wavelength dispersive spectroscopic (WDS) analysis shows the presence of both Pb and S in nearly equal molar proportions, suggesting that observed inclusions are of galena composition (Figure 4c).

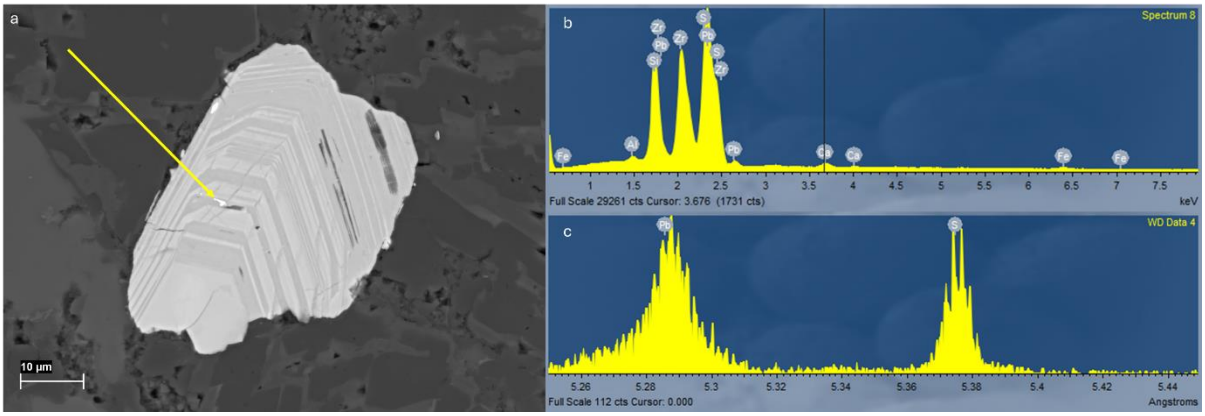

Figure 4. SEM-EDS (b) and SEM-WDS (c) analysis of galena inclusion (indicated with yellow arrow on figure a) in a zircon grain from a thin section LST12-135.4.

LA-ICP-MS dating

Concentrations of U and Pb isotopes were measured in each zircon grain. Both Wetherhill and Tera-Wasserburg concordia diagrams were plotted in MS Excel Isoplot 4.15 (Figures 6, 7, 8 and 9). Data reduction was done using Iolite 4.8.2. Most of the analyses plotted below concordia curve on the graph (Figures 6a; 7a; 8a) on a discordia line that refers to a recent low-

temperature radiogenic Pb loss or elemental fractionation, a common analytical error in microbeam dating techniques (Villa & Hanchar, 2017). The reliability of the results was evaluated based on two criteria: intensity of common lead (^{204}Pb) signal and concordance filtering (CF) based on the ratio of ^{206}Pb/^{238}U and ^{207}Pb/^{206}Pb. If the difference in final ages between the ^{206}Pb/^{238}U and the ^{207}Pb/^{206}Pb methods was more than 20%, it was considered that the data point is an outlier (disconcordant). Additionally, a concordant filter with <10% was applied for highly concordant data and in diagrams the <10% and <20% data are separately indicated. For visualization purposes, measurements from zircon grains with high ^{204}Pb concentrations were omitted because such unrealistic ages plotted far away from concordia diagram. Black ellipses on diagrams indicate unreliable age data (CF>20%). Blue data points display grains that had CF between 10% and 20%. Green data points display the most reliable data (CF<10%). The most important criteria for omitting outliers was common lead content in sample. After removing measurements based on excess ^{204}Pb, the result of concordance filter was considered.

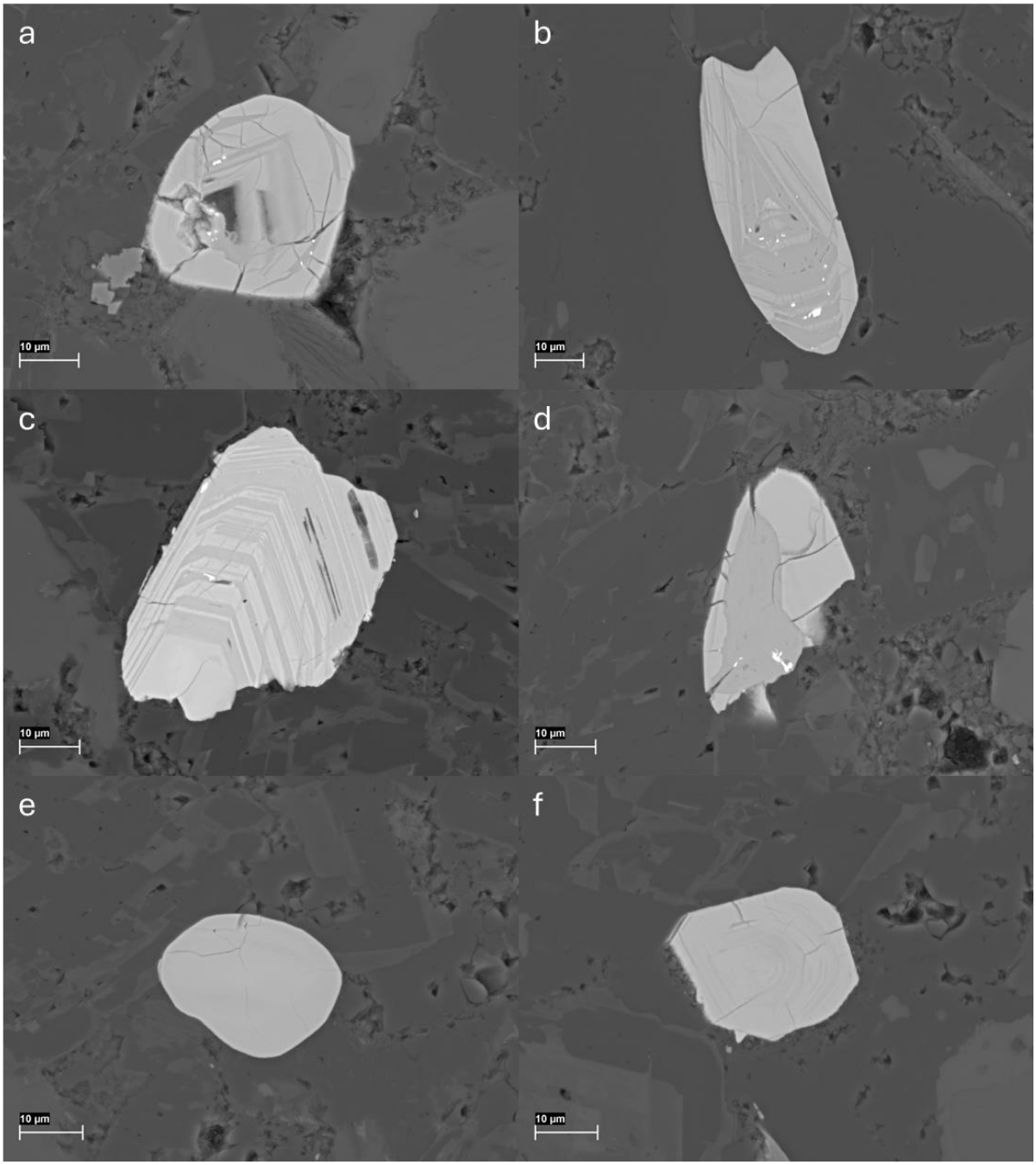

Figure 5. Zircon grains with and without galena inclusions from thin-section LST12-135.4. Galena inclusions appear as white spots in zircon grains (a-d).

Sample LST12-18.9

In total 66 zircons were measured from this sample (Appendix 1). Of those, only two were reliable under both criteria. Three of the measured grains fall into the concordance filter, which is between 10% and 20% (Figure 6). The youngest concordant grain yields Pb-Pb age of 2176.95 ± 24 Ma and the oldest yields Pb-Pb age of 2843.68 ± 26 Ma. For disconcordant grains,

principally two populations could be separated with upper intercepts at 2495 and 3109 Ma (Figure 6a). Reliable data also indicate that there are two populations of zircons – one with the age around 2.20 Ga and the other with age around 2.84 Ga (Figure 6b, c, d).

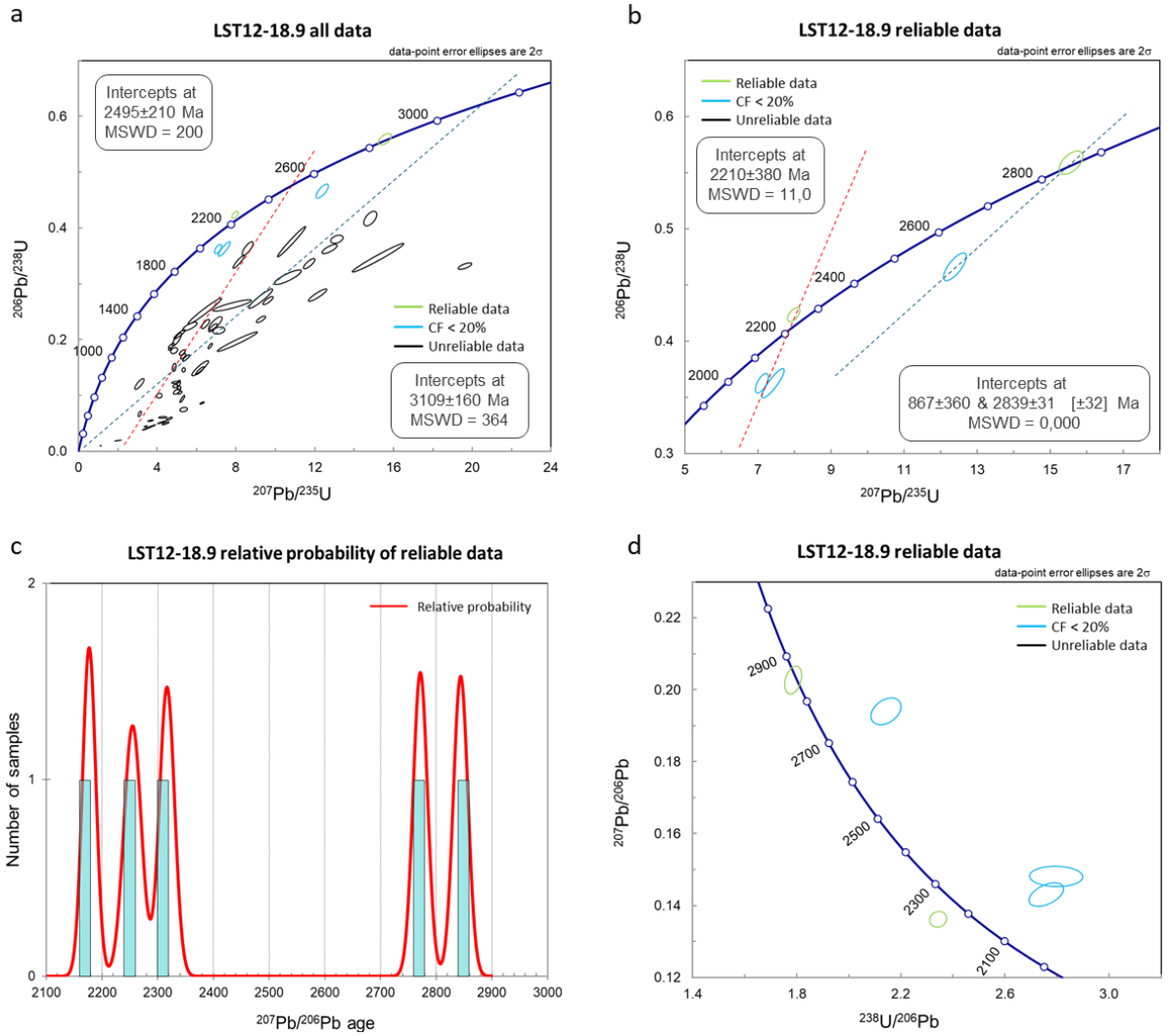

Figure 6. Data from LST12-18.9 sample. In figure (a) all acquired data without common lead contamination are shown. Dashed discordia lines on graph (a) and (b) are drawn based on the most abundant populations. In figures (b) and (d) reliable data (concordance filter <20%) is plotted on Wetherhill and Tera-Wasserburg concordia curves respectively. Figure (c) shows relative probability density of reliable data.

Sample LST12-137.0

In total 84 zircons were measured from this sample (Appendix 2). Of those, 19 were reliable under both criteria. Three were more than 10% but less than 20% from concordia (Figure 7). Reliable data yielded Pb-Pb age of 2821.22 ± 25 Ma. The relative probability density of reliable

data indicates that individual ages of zircons in this sample remain between 2.75 and 3.0 Ga, with the most probable being the age group at 2.80-2.85 Ga.

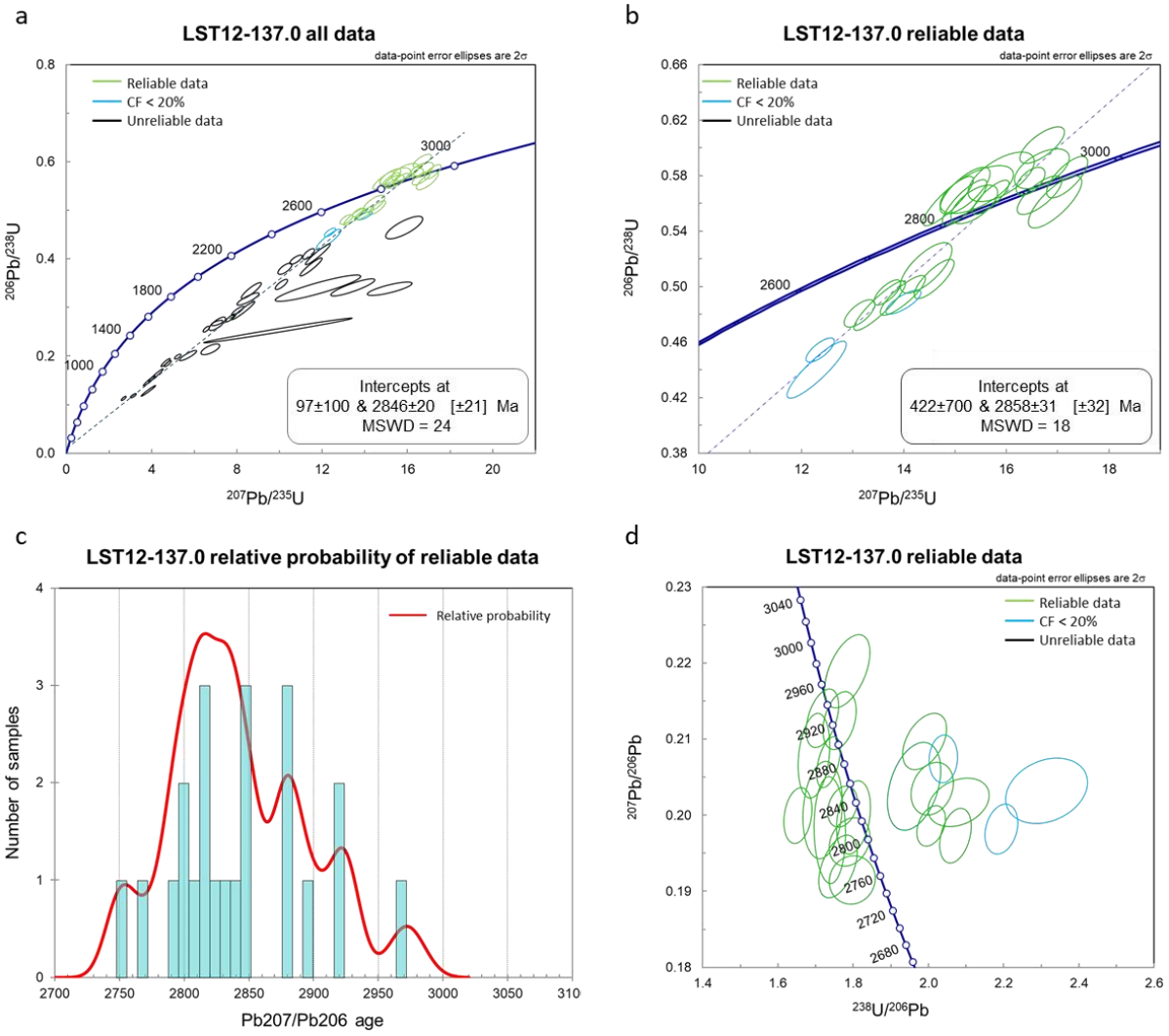

Figure 7. Data from LST12-137.0 sample. In figure (a) all acquired data with no common lead is shown. The dashed discordia line on graph (a) is drawn based on the most abundant population. In figures (b) and (d) reliable data (concordance filter <20%) is plotted on Wetherhill and Tera-Wasserburg concordia curves respectively. Figure (c) shows relative probability density of reliable data.

Sample LST12-138.7

In total 61 zircons were measured in this sample (Appendix 3). Of those, 12 were reliable under both criteria. Two analyses had concordance filter matching between 10% and 20% (Figure 8). Reliable data yielded Pb-Pb age of 2857.87 ± 31 Ma. The relative probability of reliable data indicates that individual ages of zircons in this sample remain between 2.70 and 3.50 Ga with

the most probable being the age group 2.80-2.90 Ga. But there is also a distinct population around 3.1 Ga and another around 3.5 Ga (Figure 8c).

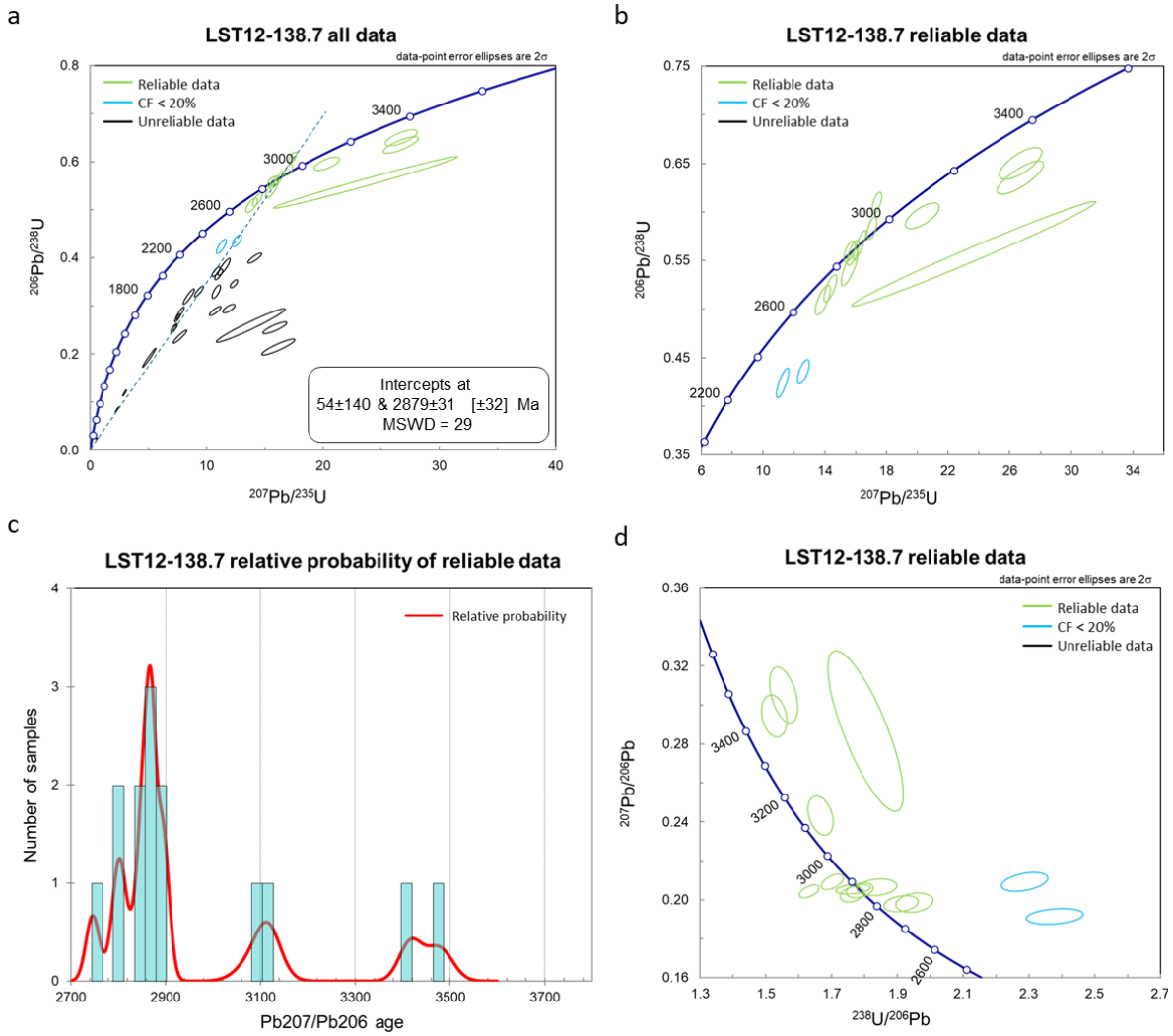

Figure 8. Data from LST12-138.7 sample. In figure (a) all acquired data with no common lead is shown. The dashed discordia line on graph (a) is drawn based on the most abundant population. In figures (b) and (d) reliable data (concordance filter <20%) is plotted on Wetherhill and Tera-Wasserburg concordia curves respectively. Figure (c) shows relative probability density of reliable data.

5. Discussion

5.1 Ages and provenance of detrital zircons in LST 12 drill core

Most of the zircon grains dated in FB/FC formation sediments in LST12 drill core yielded Archean ages, referring to zircons from crystalline basement. In the combined data of all studied samples, the most abundant population is formed by late Mesoarchean zircons 2900–2800 Ma (Figure 9), followed by Neoarchean 2800–2700 Ma zircons and small but distinct populations at ca. 3100 and ca. 3400 Ma. Only in the sample from the 18.9 m depth there was an indication of a population of 2.20 Ga age.

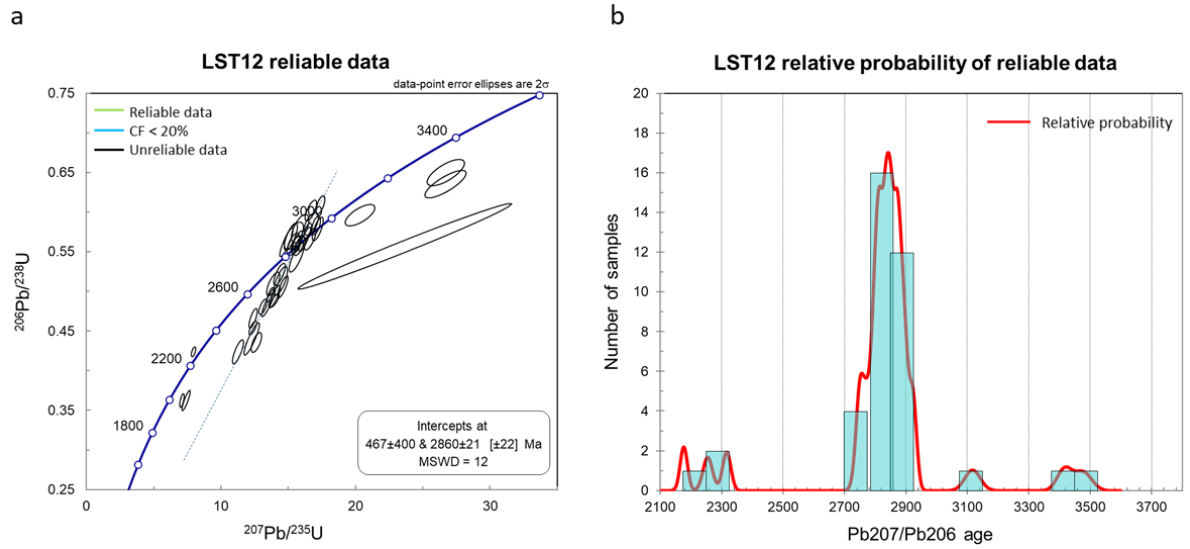

Figure 9. Reliable zircon dating data from LST12 drill core. The dashed discordia line on graph (a) is drawn based on the most abundant population and has an intersection at 2860 ± 21 Ma.

The crystalline basement in Francevillian Basin is composed mostly of Meso- to Neoarchaean (rarely Paleoproterozoic) crystalline rocks of the Archean Congo Craton (Thiéblemont et al., 2009; Weber et al., 2016). Structurally the crystalline basement of Gabon can be divided into two blocks composed of Archean granitoids and greenstone belts, and the Archean and the earliest Paleoproterozoic high-grade metamorphic terranes intruded with granitoids that were metamorphosed during the ca. 2.2–2.0 Ga Eburnaean orogeny (Ossa Ossa et al., 2020; Thiéblemont et al., 2009; Weber et al., 2016). Those blocks can be considered as sources for detrital zircons influx into the Francevillian Basin.

Indeed, Ossa Ossa et al. (2020) analysed the detrital zircons found in FA and FB units and found that most of them scatter between 2703-2635 Ma, and 2600–2618 Ma in FA and FB formations, respectively, making these formations in this sense indistinguishable. The oldest

subordinate zircon populations were of middle Mesoarchean ages between 3075 and 2900 Ma and the youngest were Neoarchean zircons between 2800–2600 Ma (Ossa Ossa et al., 2020). Similar detrital zircon ages were obtained in an earlier study of FA sandstones by Mathieu et al. (2001), whereas Bankole et al. (2018) who studied putative K-bentonites in FB formation found only detrital zircons with mean Pb-Pb age of 2971 ± 13 Ma, which were interpreted as derived from Mesoarchean crystalline basement by ascending magma.

Principally, similar Archean detrital zircon ages were found in FB/FC formation sediments in LST12, whereas most of the analysed zircons measured roughly 30-50 µm by longer axis though the zircons studied by Ossa Ossa et al. (2020) were much larger measuring >100 µm (see Figure 6 in Ossa Ossa et al., 2020). Zutterkirch et al. (2021) have suggested that large grains (>100 µm) form only a marginal part of the zircon population, and analysis of such large grains can cause bias in zircon age distributions. However, results of this study show that the size differences in dated zircons do not affect the detrital zircon age distributions in Francevillian Basin sediments. Moreover, no distinct correlation between grain size and age was noticed in LST12 dataset analysed here. All reliable zircon grains from samples LST12-137.0 and LST12-138.7 yield Archean ages as in previous studies and suggest that erosion of the Archean crystalline basement terrains or the redeposition from stratigraphically older FA and FB terrigenous sediments was the source of the detrital zircons in studied sediments.

However, a population of concordant zircons from LST12-18.9 sample giving reliable U-Pb ages at ca. 2210 Ma might indicate erosion of the ca. 2.2–2.0 Ga Eburnaean orogeny terrains as an additional source of the zircons to Francevillan Basin sediments that has not been described before (Figure 10). These zircons also can be interpreted as delimiting the maximum depositional age of the FB/FC sediments at 2210 Ma, at least in the uppermost part of the LST12 succession. In comparison, the minimum age of the FA and FB formations deposition has been so far constrained by the age of N'Goutou granitic intrusion in the Okondja sub-basin (Figure 1, 2) cross-cutting the FA and FB formations and dated by U-Pb zircon age at 2191 ± 13 Ma (Sawaki et al., 2017). The N'Goutou complex is a subvolcanic ring complex composed of three successive intrusive units (Moussavou & Minko, 2006) that were recognized by geological mapping intruding the FA and FB units and overlain by the sediments of the FC unit (Thiéblemont et al., 2014).

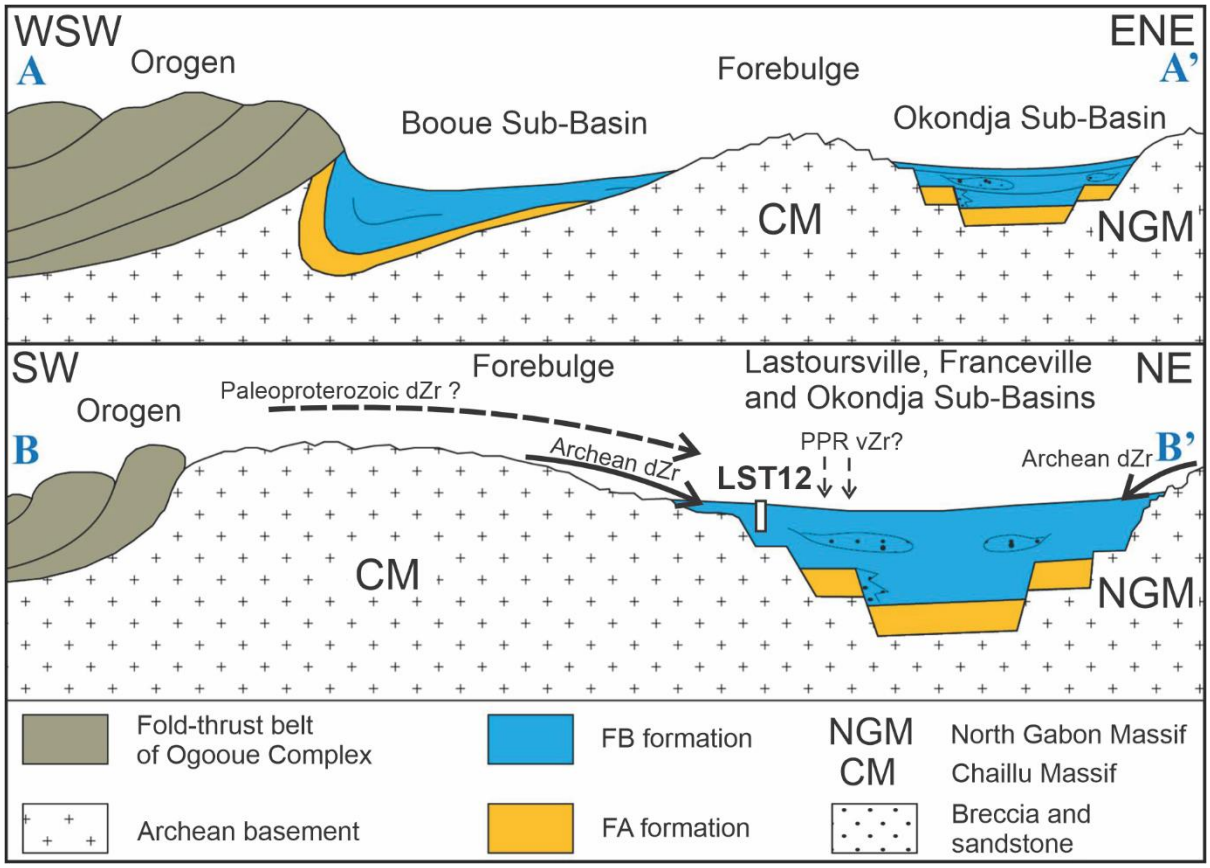

Figure 10. Schematic cross-sections of the Francevillan basin. Location of the A-A' and B-B' lines are shown in Figure 1. dZr – detrital zircon input, PPRvZr – Paleoproterozoic volcanic zircon input (modified from Thiéblemont et al., 2009; and Ossa Ossa et al., 2020).

Thus, it is possible that in addition to the Archean population from the crystalline basement and/or older FA-FB sediments, the youngest zircon in this sample with Pb-Pb age of 2176.95 ± 24 Ma was derived from the erosion of the N'Goutou Complex that has within the error a matching U-Pb zircon age at 2191 ± 13 Ma (Sawaki et al., 2017).

Alternatively, it should be considered that in Lastoursville Sub-Basin, the FB/FC deposits are succeeded by FD Formation, which begins with organic-rich black shales interlayered with pyroclastic beds that were produced by explosive volcano eruptions of andesitic to rhyolitic magmas (Weber et al., 2016).

Horie et al. (2005) dated the ignimbrites in FD formation by zircon U-Pb method at 2083 ± 6 Ma. This age was disputed by Weber et al. (2016) who noted that the sample contained two populations of zircons with different ages - one population yielded ages from 2136 to 2068 Ma and second showed ages from 2042 to 2003 Ma. The last was suggested by Weber et al. (2016) to be most possibly the true sedimentation age of tuff beds. In addition, Kuusk (2021) dated zircons from a K-bentonite bed in the FD formation shales intersected in the Doumé drill core

ca. 30 km to the east of the LST12 drill core (Figure 1). The youngest zircon in this bentonite bed yielded a reliable final Pb-Pb age of 2082 ± 19 Ma, in good agreement with Horie et al. (2005).

Most recently Paiste et al. (2024) have suggested that the uppermost part of the 139 m long LST12 and the lower part of the 76 m long Doumé cores, both cores within ~30 km of one another, share litho- and chemo-stratigraphic similarities that might indicate that LST12 units IV–VI and Doumé units I–III can partly overlap (Figure 11). This might mean that the youngest zircons measured in sample at 18.9 m in LST12 core are not all detrital but may contain instead pyroclastic zircons.

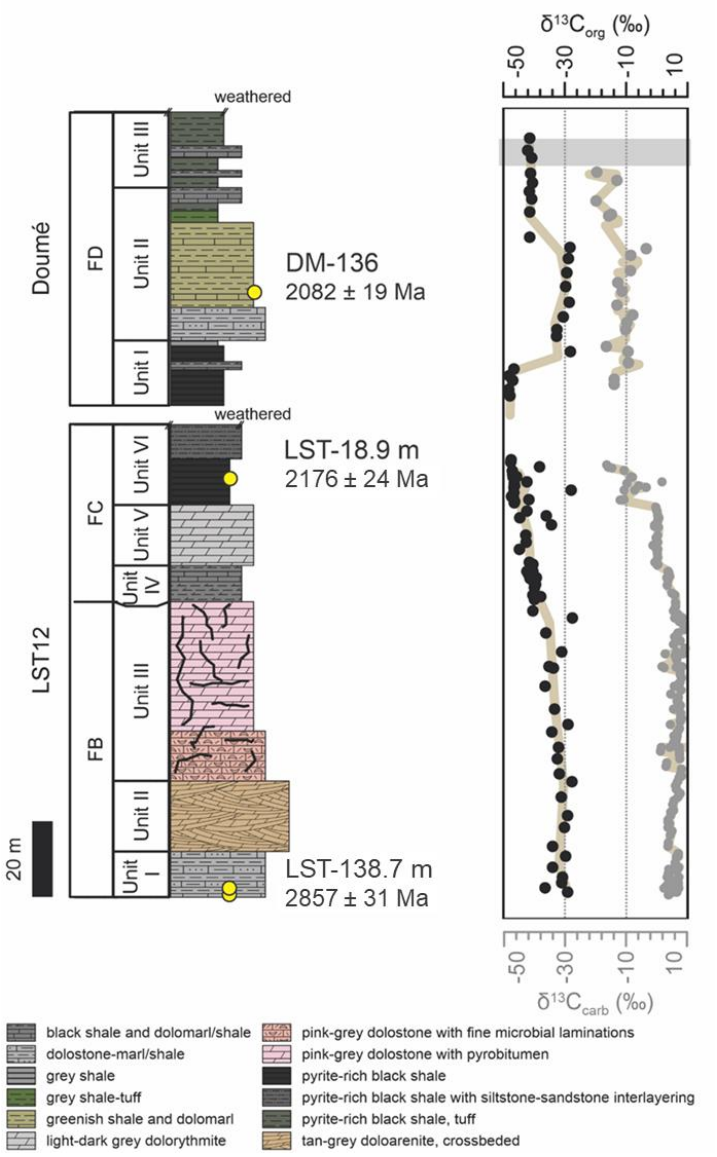

Figure 11. Schematic lithostratigraphic columns of LST12 and Doumé cores with matching organic and carbonate carbon isotope trends, and youngest ages of dated zircons. Doumé K-bentonite zircon ages from Kuusk (2021) (modified from Paiste et al., 2024)

Intriguingly, it appears that dated grains less than 10% off from concordia have noticeable morphological differences under SEM. The grains with Archean ages (Figure 12b) are rounded with smooth surfaces compared to the grain with the youngest Pb-Pb age (Figure 12a), showing angular habitus, implying that all Archean zircons are undoubtedly through several redeposition cycles and detrital, while the youngest grain could be of pyroclastic origin. However, in comparison of the grains in the same sample with a larger offset from concordia but within 20% do not support this hypothesis as all three grains, two of which with Archean ages, were rather similar to the youngest concordant grain (Figure 12c, d). This indicates that the concordant grains are all from similar origin and supports the hypothesis of detrital zircons from two different source deposits. Nevertheless, it remains unclear whether the source of the youngest zircon population was the ca. 2.2–2.0 Ga Eburnaean orogeny rocks or the 2191 ± 13 Ma N'Goutou Complex granitoids.

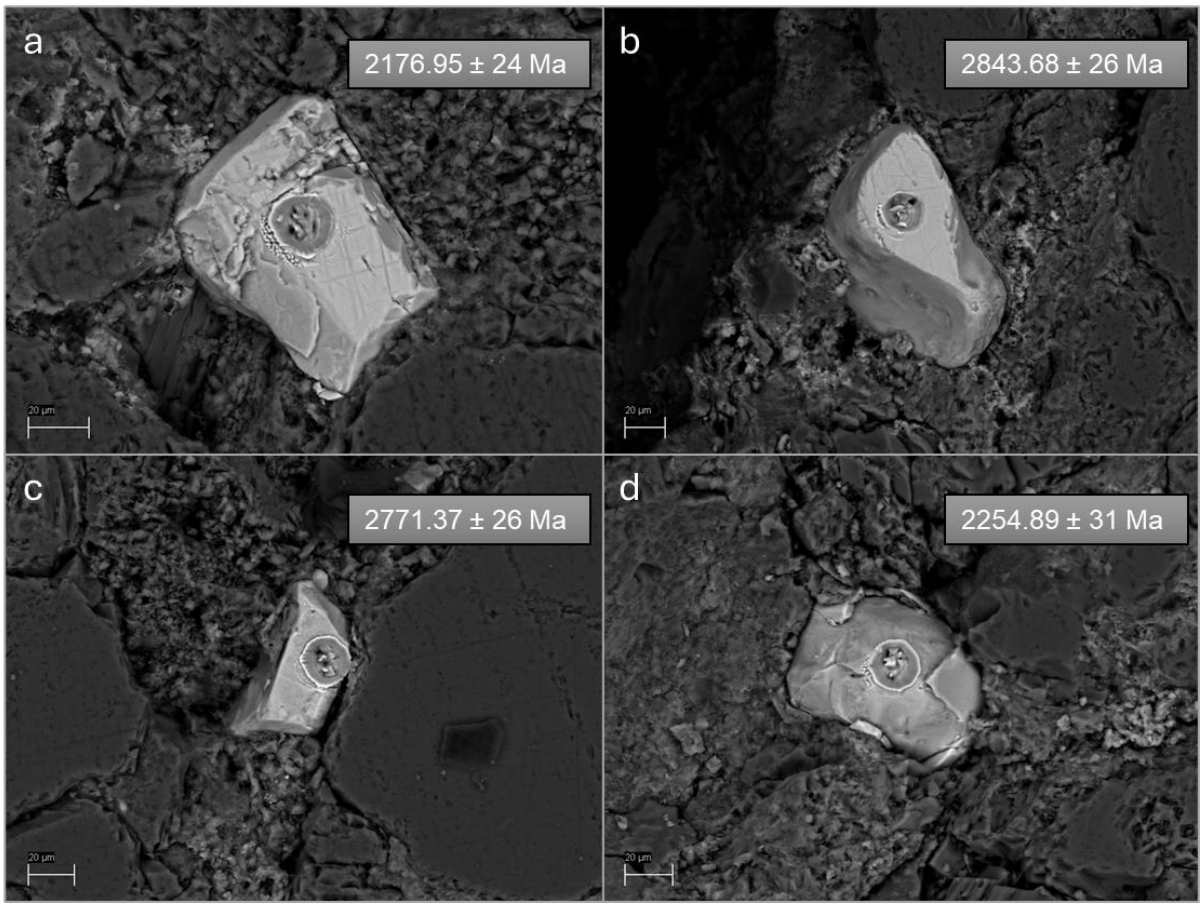

Figure 12. Zircon grains from LST12-18.9 sample after laser ablation. Reliable Pb-Pb ages are presented for each sample. Grains (a) and (b) were concordant while (c) and (d) were within 20% from concordia.

5.2 Origin of galena inclusions in zircons

Samples LST12-136.0; LST12-136.8; LST12-138.0 contained abundant zircons with galena inclusions. In most cases, the inclusions were located in growth zones of zircon grains, but occasionally the cores were affected, too.

Such grains were not suitable for U-Pb dating as lead concentrations would not be related to the age of the grains. However, as lead should not be able to enter into zircon crystal structure during its crystallization and galena does not crystallize typically with zircon then it remains unclear why those zircons frequently contain galena inclusions.

This phenomenon was noted already by Mathieu et al. (2001) who described galena inclusions in zircons from coarse-grained sandstones of Franceville Sub-Basin FA formation. They also found that zircon cores did not contain galena and inclusions were mainly at the rims aligned along the growth zone boundaries. The cores of such zircons yielded Archean ages, which was confirmed by (Ossa Ossa et al., 2020) who concluded that zircons in FA formation derive from crystalline basement, whereas zircons in FB formation originate from both Archean basement and reworked earlier-deposited sediments in the basin.

Mathieu et al. (2001) related the galena formation in zircons to the intensive hydrothermal leaching. There were two important tectonic events since the deposition of Francevillian succession regarding potential Pb mobilization (Gauthier-Lafaye & Weber, 2003; Mathieu et al., 2001). First, Eburnaean orogeny (ca 2.0 – 2.2 Ga ago) that only affected Francevillian Basin mildly, but it has been considered as initiating the first uranium redeposition by forming a network of fractures that linked various aquifers and inducing waterflow within the basin. After that, ca. 1000 million years later, about 970 Ma ago there was an extensional event where dolerite dykes formed in Franceville Sub-Basin (Bonhomme et al., 1982 *cit.* Gauthier-Lafaye & Weber, 2003). This event is believed to be linked to the redistribution of Pb, U and light rare earth elements (LREE) in the basin (Gauthier-Lafaye & Weber, 2003; Mathieu et al., 2001). The model suggested by Mathieu and others (2001) suggests that dissolution of zircons occurred at ca. 2000 Ma, producing a porous and distorted crystal structures which has allowed a later incorporation of Pb whereas galena inclusions in altered zircons located in the vicinity of the Oklo natural reactors (<20 m from reactor zones) had radiogenic lead compositions but galena inclusions in altered zircon rims located far from reactor zones have non-radiogenic Pb isotopic compositions showing the external origin of lead. However, it was considered that the

timing of galena crystallization in zircons was the same, both near and far from reaction zones. (Mathieu et al., 2001)

It is important that LREEs and Pb are considered relatively immobile, but they could be mobilized from monazite and other minerals in highly saline brines at 135-155 °C and 1000 bar (Mathieu et al., 2000). Previous studies have not described strong hydrothermal alteration in Lastoursville Sub-Basin, though the discovery of numerous zircon crystals with galena inclusions in LST12 sediments would suggest that the Lastoursville Sub-Basin was flushed by hydrothermal fluids similar to the Francevillian Sub-Basin. Principally, it might be possible that zircons with galena inclusions could have been re-deposited from FA formation of Franceville Sub-Basin to Lastoursville Sub-Basin after galena crystallization. However, this does not agree with the proposed timing of the galena crystallization event at ca. 970 Ma (Mathieu et al., 2001). So far, it has been considered that the whole sedimentary succession in Francevillian Basin is older than 2.0 Ga, thus galena crystallization in zircon grains around 1000 Ma ago and later redeposition of these grains would not agree with this model.

Alternatively, Mathieu and others (2001) suggested another model where zircons originate from a very old crystalline basement that is of 3.7 Ga age and have been altered around 2.0 Ga ago during the Eburnaean orogeny. However, they rejected this model because no basement that old has been described in Francevillian Basin and it would have been geochemically difficult to explain conditions where uranium leaching, and galena crystallization would simultaneously be possible. Another plausible explanation is that the tectonic events described in Franceville Sub-Basin had a much wider alteration zone and affected other sub-basins as well, creating geochemical conditions favourable for Pb leaching and subsequent galena crystallization in zircons. It must be underlined that such intensive alteration with pervasive fluids has important implications for the preservation and nature of the trace-element and isotopic signals in the Francevillian Basin sediments that have been considered as the best-preserved Paleoproterozoic sedimentary rocks (Gauthier-Lafaye & Weber, 2003) potentially holding valuable information for understanding the post-GOE environmental changes.

Summary

The aim of this master thesis was, first, to test the applicability of the *in situ* zircon U-Pb dating technique on small zircon grains from carbonate and black-shale rocks and, second, to refine the maximum depositional ages of the Paleoproterozoic sediments in the FB/FC formations of the Francevillian Basin.

Detrital zircons have proven to be a reliable method of provenance and age studies as zircons are rather resistant to any chemical or physical alterations. However, the traditional method of dating zircons has many steps in the sample collecting and preparation process that might bias the results. In this study laser-ablation inductively coupled plasma mass-spectrometry (LA-ICP-MS) measurements were conducted *in situ* to minimize the effects of sample preparation.

Seven samples from LST12 drill core intervals where zircon concentration was more than 400 ppm were chosen for analysis. Three of them: LST12-18.9; LST12-137.0 and LST12-138.7 contained zircons that were suitable for dating by LA-ICP-MS.

Zircons from the drill core yielded mainly Archean ages with the most dominant population around 2860 Ma. This implies that zircons originate from the surrounding crystalline basement and agree well with previous studies. However, a population of around 2200 Ma that was found in LST12-18.9 sample indicates an additional source of the detrital zircons derived either from the erosion of ca. 2.2–2.0 Ga Eburnaean orogeny rocks or the 2191 ± 13 Ma N'Goutou Complex granitoids. There was no apparent correlation between the morphology of the grains in different age groups suggesting that the dominant source for detrital zircons in Francevillian Basin was the erosion of the Archean crystalline basement and there were no other detrital zircon sources that would have provided smaller grains with a different age spectrum. Overall, it must be concluded that in situ U-Pb dating is a viable method for small zircon grains even in carbonate and shale sediments not typically studied for detrital zircons.

Most of the studied LST-12 samples contained zircons with galena inclusions in them. Mathieu et al. (2001) described galena inclusions in Francevillian Sub-Basin zircons and suggested that the excess lead was mobilized around 1000 Ma ago during Franceville Sub-Basin regional extension. Results of this study show that galena inclusions are present also in zircons Lastoursville Sub-Basin FB-FC formation suggesting a wider influence of zircon leaching and galena precipitation in hydrothermal events.

Francevillian Basin has so far been considered one of the best-preserved Paleoproterozoic sedimentary successions in the world and has thus been extensively studied by geologists. Indications of hydrothermal fluid alterations in the basin suggest that caution should be applied when using geochemical and trace element data to interpret post-GOE environmental changes.

Detriitsete tsirkoonide dateerimine *in situ* U-Pb meetodil Gaboni Franceville'i settebasseini Lastoursville'i alambasseini karbonaatsetest kihtidest ja mustadest kiltadest

Carmel Kuusk

Kokkuvõte

Selle töö eesmärk oli dateerida väiksemaid kui 100 µm detriitseid tsirkooniterasid *in situ* U-Pb meetodil Paleoproterosoikumi Franceville'i settebasseini (Gabon) Lastoursville'i alambasseini LST12 puursüdamiku karbonaatsetest kihtidest ja mustadest kiltadest ning ühtlasi täpsustada antud läbilõikes avatud FB-FC kihtide maksimaalset (settimis-)vanust.

Detriitseid tsirkoone on laialdaselt kasutatud terrigeensete setete päritolu kirjeldamiseks. Nende dateerimise abil on võimalik hinnata lisaks settematerjali päritolule ka selle vanust ja settimisaega. Tsirkoonid on vastupidavad nii füüsikalisele kui keemilisele murenemisele ja neid on võimalik dateerida U-Pb meetodil. Traditsioonilised tsirkoonide dateerimise meetodite kasutamisel tsirkoonid separeeritakse ümbriskivimist mitmes proovi ettevalmistamise etapis, kus iga samm võib saadavaid tulemusi mõjutada. Ebausaldusväärsuse vähendamiseks dateeriti selles töös tsirkoone lihvitud kivimipalades *in situ* laser-ablatsiooni induktiivsidestatud plasma massi-spektromeetria (LA-ICP-MS) abil.

Üldkeemiliste analüüside alusel valiti LST12 puursüdamikust neli intervalli, kus tsirkooni sisaldus oli üle 200 ppm. Nende intervallide proovidele tehti röntgenfluorestsents analüüsid ja valiti seitse intervalli edasiseks uurimiseks – 18,9 m, 57,5 m, 136,0 m, 136,8 m, 137,0 m, 138,0 m ja 138,7 m. Neis kõigis oli Zr sisaldus üle 400 ppm, mille põhjal võis eeldada, et seal leidub dateerimiseks sobivaid tsirkooniterasid.

Kolmes proovis – LST12-18.9, LST12-137.0 ja LST12-138.7 olid dateerimiseks sobivad tsirkooniterad. Nende U ja Pb isotoopide sisaldust mõõdeti LA-ICP-MS abil ja selle põhjal arvutatud vanuseid kujutati konkordiadiagrammidel. Selgus, et enamus teradest on Arhaikumi vanusega ja kõige sagedasema populatsioon moodustasid terad ca. 2860 Ma vanusega. LST12-18.9 proovist leiti ka populatsioon, mille konkordiavanus oli ca. 2200 Ma, mida ei ole varem Franceville'i Basseini setetest kirjeldatud. Nende nooremate tsirkooniterade morfoloogia ei erinenud vanematest ligikaudu konkordsetest detriitsetest teradest, mille põhjal võib järeldada, et ka noorema populatsiooni moodustavad detriitsed terad kuigi eksisteerib võimalus, et need

on püroklastilised. Nende tsirkoonide päritolu ei ole üheselt selge ning need võivad pärineda kas ca. 2.2–2.0 Ga Eburniani orogeense kompleksi kivimitest või 2191 ± 13 Ma N'Goutou intrusiivsete granitoidide kompleksist.

Paljud leitud tsirkooniterad sisaldasid galeniidi (PbS) suletisi, mistõttu need ei sobinud U-Pb dateerimiseks, sest plii sisaldus ei ole neis seotud terade vanusega.

Üldkokkuvõtteks saab väita, et Franceville'i Basseini setetes ei ole väikesemõõdulisi (<100 µm) tsirkooniterasid, mis võiksid olla suurtest teradest põhimõtteliselt erineva vanusespektriga. Samuti võib järeldada, et *in situ* U-Pb dateerimine on arvestatav meetod väikeste tsirkooniterade dateerimiseks isegi karbonaatsetes setetes ja kiltades-savikivimites, mida tavaliselt detriitsete tsirkoonide uuringutes ei kasutata.

Mathieu ja teised (2001) kirjeldasid sama nähtust Franceville'i alambasseini FA kihi jämedateralistes liivakivides esinenud tsirkoonides. Nad hindasid, et tsirkoonide leostumine on seostatav ligikaudu 2000 Ma toimunud Eburnaeani orogeneesiga, mis mõjutas ka Franceville'i settebasseini. Plii mobiliseerumise ja galeniidi suletiste tekkimine tsirkoonides toimus arvatavasti ca 1000 Ma tagasi kõrge soolsusega ja ca 150 °C temperatuuriga fluidide sissetungimisel, mis on arvatavasti laiema mõjuga kui ainult Franceville'i alam-bassein ning ulatusid ka Lastoursville'i alam-bassini setenditesse.

Franceville'i settebasseini on seni peetud üheks paremini säilinud Paleoproterosoikumi-aegseks settebasseiniks maailmas. Samas ilmneb, et intensiivsete hüdrotermaalsete protsesside mõju basseinis on laialdane ning on arvatavasti jätnud oma jälje erinevatele (isotoop-)geokeemilistele settimisaegse keskkonna tingimusi kirjeldavatele indikaatoritele.

Acknowledgements

I would like to thank my supervisor for guidance throughout the whole study and everyone else who helped on the way – Marian Külaviir for the help with SEM, Peeter Paaver and Päärn Paiste for the help with LA-ICP-MS analyses and data reduction.

Appendix 1

Table 2. Analyses from sample LST12-18.9.

Grain	ppm U	Th	Pb	U/Th	Pb206/U238	2 SE	Pb207/U235	2 SE	Pb207/Pb206	2 SE	Age (Ma) Pb206/U238	2 SE	Age Pb207/U235	2 SE	Age (Ma) Pb207/Pb206	2 SE
18.9-1	819.529	425.089	443.471	1.872	0.210	0.006	5.136	0.238	0.177	0.004	1224.567	33.679	1833.006	37.889	2615.372	32.248
18.9-2	0.000	0.000	-0.508	0.000	102.296	1281.664	-103906.715	129011.476	-1.336	2.343	54855.220	1038.452	12887.298	200.425	3443.829	440.173
18.9-3	62.918	38.370	47.821	1.624	0.559	0.008	15.569	0.269	0.203	0.003	2859.330	34.861	2846.826	16.528	2843.685	26.141
18.9-4	560.641	629.034	859.500	0.837	0.312	0.011	10.635	0.572	0.243	0.008	1742.882	52.106	2453.874	51.067	3113.651	51.029
18.9-5	866.106	448.257	493.576	1.917	0.228	0.007	6.461	0.158	0.205	0.003	1321.386	34.514	2033.824	21.510	2861.720	26.130
18.9-6	1200.504	2721.645	954.871	0.459	0.105	0.002	5.153	0.100	0.357	0.006	643.284	14.242	1840.751	16.855	3738.100	27.561
18.9-7	519.255	406.334	350.171	1.235	0.177	0.004	5.273	0.130	0.217	0.004	1049.283	21.535	1861.204	21.211	2951.801	30.692
18.9-8	579.643	311.228	267.215	2.005	0.376	0.022	10.830	0.591	0.211	0.003	2030.923	107.535	2468.465	56.142	2909.413	22.100
18.9-9	1262.198	167431.345	153410.673	0.007	0.409	0.009	7.677	0.199	0.136	0.001	2208.084	39.494	2186.846	22.074	2172.604	17.204
18.9-10	2398.369	714.492	1717.816	4.218	0.094	0.005	5.280	0.097	0.429	0.013	576.072	30.450	1862.250	15.307	3986.473	51.894
18.9-11	1387.712	1819.248	1117.886	0.734	0.122	0.004	5.094	0.069	0.313	0.010	738.647	24.726	1833.108	11.577	3510.154	50.032
18.9-12	0.000	0.000	4.709	0.000	-29597.757	7169.492	-3549621.802	675134.821	1.419	0.325	36347.001	14809.976	10301.177	2796.497	3923.979	274.901
18.9-13	3789.728	1338.109	1889.278	2.752	0.045	0.001	3.418	0.057	0.556	0.007	281.568	5.609	1506.007	13.300	4393.309	18.573
18.9-14	123.157	54.536	37.812	2.243	0.200	0.009	4.998	0.192	0.187	0.005	1171.767	49.847	1813.084	33.816	2690.973	45.887
18.9-15	1128.264	894.643	734.547	1.338	0.150	0.006	4.858	0.075	0.245	0.010	900.173	35.016	1792.810	12.917	3110.962	65.518
18.9-16	391.639	341.113	493.869	1.079	0.270	0.006	9.628	0.207	0.261	0.003	1537.321	31.263	2397.676	20.398	3245.132	20.763
18.9-17	819.392	1011.174	671.921	0.760	0.167	0.005	5.474	0.141	0.239	0.004	994.778	26.446	1889.817	21.334	3105.781	24.545
18.9-18	6349.350	2006.665	2473.943	2.541	0.043	0.004	3.589	0.267	0.665	0.020	267.424	24.644	1488.571	65.767	4624.170	43.358
18.9-19	797.514	645.874	584.214	1.223	0.236	0.005	9.266	0.191	0.285	0.004	1366.452	24.737	2359.432	19.026	3384.996	21.984
18.9-20	9412.859	3615.307	2921.108	2.455	0.019	0.001	2.015	0.139	0.737	0.016	123.163	6.198	1089.317	47.346	4767.588	31.037
18.9-21	1106.163	930.588	854.183	1.140	0.189	0.004	6.700	0.095	0.258	0.003	1113.322	20.066	2070.356	12.477	3234.869	19.150
18.9-22	269.084	337.251	355.526	0.764	0.424	0.005	7.970	0.138	0.136	0.002	2276.473	23.082	2224.218	15.483	2176.948	23.871
18.9-23	1034.812	125.629	382.036	7.882	0.183	0.002	4.637	0.057	0.184	0.002	1082.976	10.688	1755.863	10.694	2685.040	18.376
18.9-24	482.216	458.597	1380.343	1.002	0.332	0.005	19.622	0.281	0.429	0.005	1845.910	22.132	3070.306	13.905	4009.704	16.476
18.9-25	1599.969	2072.596	1300.588	0.780	0.113	0.003	5.112	0.085	0.332	0.008	690.928	15.613	1835.190	14.217	3613.349	38.322
18.9-26	1394.038	319.997	536.482	5.735	0.096	0.002	2.868	0.203	0.221	0.018	590.085	12.610	1334.672	50.340	2838.973	115.332
18.9-27	137.086	87.115	135.945	1.532	0.466	0.010	12.391	0.258	0.194	0.003	2463.721	44.355	2634.316	20.549	2771.374	25.818
18.9-28	1222.486	1387.597	956.227	0.891	0.149	0.011	6.194	0.350	0.319	0.013	886.932	60.234	1971.906	47.700	3526.367	59.527
18.9-29	296.153	177.448	190.037	1.605	0.362	0.011	7.405	0.251	0.148	0.002	1988.200	50.150	2149.118	30.311	2316.606	27.130
18.9-30	0.018	0.034	10.511	0.300	2.03165E+14	5.05547E+13	2.26024E+16	6.63636E+15	0.964	0.142	186715.127	12255.206	34126.888	1941.246	4085.938	201.798
18.9-31	455.635	449.229	794.625	0.960	0.336	0.007	11.718	0.240	0.253	0.003	1864.746	34.837	2579.531	18.827	3199.969	20.513
18.9-32	194.086	213.808	290.114	0.870	0.362	0.007	7.094	0.146	0.143	0.003	1991.265	33.212	2118.712	18.448	2254.889	31.310
18.9-33	1243.809	239.167	840.434	5.036	0.123	0.002	4.930	0.155	0.290	0.009	749.530	10.599	1797.139	26.714	3392.659	45.394
18.9-34	2061.874	2409.651	2047.094	0.816	0.075	0.003	5.346	0.154	0.534	0.020	465.086	17.330	1867.711	23.791	4302.753	58.040
18.9-35	426.259	255.488	600.869	1.628	0.362	0.007	12.743	0.316	0.255	0.004	1990.465	33.430	2652.931	23.232	3206.462	23.911
18.9-36	964.684	249.914	362.400	3.973	0.251	0.019	6.409	0.699	0.173	0.006	1422.225	96.514	1909.424	91.174	2557.269	54.710
18.9-37	3667.587	5016.392	2908.460	0.744	0.058	0.002	4.617	0.122	0.590	0.015	364.078	14.268	1748.076	22.477	4467.254	37.141

Grain	ppm U	Th	Pb	U/Th	Pb206/U238	2 SE	Pb207/U235	2 SE	Pb207/Pb206	2 SE	Age (Ma) Pb206/U238	2 SE	Age Pb207/U235	2 SE	Age (Ma) Pb207/Pb206	2 SE
18.9-38	1469.740	170.372	1081.344	10.058	0.197	0.014	8.066	0.829	0.282	0.010	1143.908	76.850	2115.226	91.837	3335.491	58.678
18.9-39	366.299	173.139	552.947	2.092	0.417	0.010	14.813	0.265	0.261	0.005	2240.889	47.435	2799.123	16.947	3238.182	32.709
18.9-40	812.127	545.928	657.568	1.473	0.216	0.005	7.133	0.250	0.243	0.009	1260.858	28.407	2119.982	30.875	3105.010	57.077
18.9-41	3799.806	8190.284	3125.486	0.456	0.050	0.002	4.434	0.146	0.652	0.014	313.433	12.976	1707.848	27.370	4612.960	30.735
18.9-42	765.075	160.182	547.186	4.630	0.261	0.008	7.812	0.792	0.207	0.015	1490.406	43.067	2108.530	85.570	2759.981	110.151
18.9-43	0.028	0.088	4.506	0.032	-3647.408	809.337	-499274.440	90052.057	0.663	0.502	20029.073	7051.149	5067.968	373.866	3921.017	296.695
18.9-44	1077.460	965.605	834.661	1.043	0.144	0.006	6.170	0.183	0.316	0.007	866.310	34.660	1990.125	27.025	3542.810	32.993
18.9-45	1047.910	1448.485	843.815	0.727	0.151	0.003	3.928	0.163	0.192	0.010	906.563	15.130	1605.106	33.910	2696.618	81.646
18.9-46	1296.092	882.651	1077.329	1.427	0.117	0.002	4.917	0.108	0.308	0.008	712.889	13.852	1800.151	18.895	3490.249	42.211
18.9-47	324.701	294.991	215.845	1.095	0.224	0.006	5.667	0.301	0.183	0.006	1298.254	32.493	1908.633	41.314	2657.212	47.852
18.9-48	0.008	0.094	3.169	0.000	-2877585.864	1021751.068	-307406880.3	85583194.57	0.138	0.391	66040.938	10830.362	12918.112	3207.421	4034.248	265.891
18.9-49	973.973	117.497	367.221	8.532	0.180	0.004	4.859	0.146	0.197	0.006	1068.388	22.966	1786.418	25.819	2774.956	50.900
18.9-50	0.012	0.345	-0.015	0.040	-1074228.178	4639473.979	20692711.35	373995099.3	0.182	0.473	102632.618	1647.246	20855.597	884.029	3506.081	535.958
18.9-51	2974.559	16886.283	1820.448	0.172	0.055	0.001	3.659	0.107	0.482	0.010	345.323	6.261	1554.954	24.049	4174.789	34.285
18.9-52	3163.080	1069.610	2151.847	3.322	0.061	0.001	4.283	0.171	0.510	0.020	379.813	7.516	1673.136	34.132	4225.281	65.315
18.9-53	1937.359	994.771	1083.654	2.293	0.099	0.003	4.102	0.111	0.310	0.015	609.854	20.502	1647.622	22.005	3475.495	69.607
18.9-54	251.567	86.662	75.282	3.245	0.364	0.010	8.604	0.224	0.173	0.003	1994.539	45.970	2292.315	24.135	2585.319	29.777
18.9-55	14866.837	6278.691	2795.414	2.237	0.010	0.000	1.120	0.023	0.782	0.007	66.565	1.476	761.243	10.629	4879.078	12.703
18.9-56	1651.531	671.196	1121.499	2.820	0.103	0.002	4.705	0.182	0.332	0.014	634.938	9.881	1756.137	29.321	3590.376	59.108
18.9-57	335.669	187.369	504.166	1.734	0.380	0.006	13.121	0.261	0.251	0.005	2072.787	28.539	2683.280	18.864	3183.783	32.616
18.9-58	281.029	142.553	876.738	1.841	0.601	0.016	24.549	1.961	0.291	0.017	3023.597	62.031	3225.332	72.907	3343.062	84.127
18.9-59	2446.031	1057.171	2342.587	2.161	0.086	0.002	6.285	0.093	0.531	0.006	532.660	9.141	2013.901	13.010	4325.410	17.843
18.9-60	1882.452	2025.187	1031.480	0.929	0.107	0.004	4.997	0.146	0.348	0.012	654.278	24.626	1810.921	24.540	3672.979	51.037
18.9-61	1296.706	1099.818	740.024	1.233	0.146	0.003	5.346	0.077	0.268	0.007	875.977	17.570	1873.965	12.255	3287.191	39.425
18.9-62	473.564	516.848	707.039	0.898	0.347	0.021	15.216	1.065	0.314	0.005	1899.543	99.651	2770.540	67.918	3534.119	25.251
18.9-63	3.888	6.706	417.835	0.673	5.621	0.244	692.683	30.464	0.895	0.014	12125.617	254.647	6626.359	47.299	4933.429	15.725
18.9-64	258.473	138.701	134.958	1.798	0.221	0.006	6.831	0.172	0.225	0.004	1286.009	30.320	2083.253	22.550	3009.324	25.385
18.9-65	679.495	568.721	462.584	1.134	0.170	0.004	5.322	0.116	0.228	0.004	1012.275	21.373	1867.391	18.545	3028.927	25.959
18.9-66	577.036	295.811	216.191	1.954	0.340	0.010	8.148	0.235	0.174	0.002	1879.780	46.511	2240.822	26.158	2596.890	18.254
18.9-67	257.796	201.396	107.671	1.310	0.121	0.008	3.102	0.187	0.194	0.007	729.572	45.510	1406.643	44.736	2747.112	58.996
18.9-68	728.122	325.279	321.884	2.174	0.229	0.010	6.965	0.281	0.220	0.005	1331.873	51.726	2098.120	34.099	2968.037	36.413
18.9-69	1881.690	884.642	1254.475	2.050	0.052	0.002	4.222	0.173	0.586	0.008	328.237	12.638	1662.315	32.858	4468.926	19.117
18.9-70	777.994	638.489	495.027	1.181	0.189	0.003	4.724	0.118	0.182	0.003	1116.864	18.009	1768.263	21.183	2658.532	28.054
18.9-71	0.000	0.008	1.630	0.000	-7373609.285	3156332.706	-1140132102	362118547.5	0.446	0.378	83474.836	11400.101	16453.610	2653.989	3421.355	328.893
18.9-72	625.200	471.866	804.850	1.300	0.280	0.009	12.148	0.379	0.316	0.004	1586.727	46.258	2601.612	32.286	3543.686	21.865
18.9-73	657.464	228.699	431.945	2.545	0.273	0.014	9.258	0.501	0.247	0.004	1545.793	73.253	2321.400	57.362	3153.232	28.789
18.9-74	2824.898	3366.594	1208.615	0.833	0.067	0.004	3.110	0.070	0.359	0.018	416.351	22.998	1430.755	17.219	3700.300	70.908

Appendix 2

Table 3. Analyses from sample LST12-137.0.

Grain	ppm U	Th	Pb	U/Th	Pb206/U238	2 SE	Pb207/U235	2 SE	Pb207/Pb206	2 SE	Age (Ma) Pb206/U238	2 SE	Age (Ma) Pb207/U235	2 SE	Age (Ma) Pb207/Pb206	2 SE
137a-1	0.729	135.735	158.500	0.005	1.701	0.321	153.284	26.973	0.700	0.069	5775.998	607.248	4878.779	156.716	4321.640	109.644
137a-2	0.000	0.000	6.629	6.60887E+11	-3320466.108	837723.9806	-443554824.4	109648152.1	0.926	0.281	59427.903	21600.490	5555.803	1322.311	4162.566	187.952
137a-3	11.143	85.216	458.475	0.136	1.927	0.068	205.923	7.358	0.770	0.014	6922.596	159.321	5408.265	35.778	4823.182	23.493
137a-4	995.740	1977.443	363.162	0.485	0.187	0.007	4.655	0.172	0.181	0.003	1102.790	36.300	1747.097	29.509	2657.671	24.844
137a-5	622.629	939.810	257.373	0.827	0.267	0.011	7.076	0.319	0.188	0.004	1516.792	56.136	2099.515	40.891	2717.309	31.153
137a-6	561.134	1313.064	611.599	0.421	0.279	0.007	7.713	0.194	0.201	0.003	1583.748	33.659	2191.759	23.011	2826.450	21.238
137a-7	190.398	210.576	196.602	0.911	0.464	0.019	15.858	0.714	0.250	0.007	2455.659	83.612	2862.223	43.888	3179.721	47.080
137a-8	24.342	2277.411	1747.447	0.014	0.926	0.028	65.283	2.455	0.509	0.010	4207.546	94.272	4240.066	37.657	4260.669	31.191
137a-9	0.000	0.000	98.480	918477296.3	3107702.796	584176.3295	423749629.5	83368580.7	0.958	0.032	94869.834	1055.593	19893.574	164.590	4841.551	39.923
137a-10	572.248	1667.264	1123.039	0.337	0.339	0.011	15.162	0.861	0.326	0.012	1877.933	53.063	2811.046	53.168	3585.159	56.644
137a-11	179.125	303.478	132.033	0.596	0.380	0.010	10.251	0.269	0.198	0.004	2073.567	44.351	2457.609	22.863	2806.155	32.750
137a-12	132.664	78.963	104.741	1.681	0.585	0.012	16.689	0.436	0.208	0.005	2965.972	47.344	2912.531	24.995	2881.056	36.359
137a-13	48.964	69.374	87.687	0.691	0.579	0.015	15.893	0.529	0.201	0.005	2940.487	59.283	2863.061	31.780	2821.223	43.336
137a-14	170.708	273.201	209.971	0.736	0.561	0.015	16.944	0.424	0.219	0.004	2864.452	63.155	2926.449	23.933	2971.871	27.569
137a-15	390.857	1923.877	1214.058	0.198	0.269	0.063	20.833	7.113	0.462	0.046	1282.377	179.801	2648.298	201.449	3783.704	94.727
137a-16	0.056	0.351	4.799	2932518.955	121612.2826	43520.06109	14970146.4	3719593.435	0.609	0.377	55682.857	7034.380	13680.025	1158.932	3502.630	343.288
137a-17	165.084	171.485	101.924	1.025	0.506	0.012	14.587	0.317	0.210	0.003	2633.266	49.697	2783.461	21.046	2897.782	23.467
137a-18	267.696	406.753	67.399	0.677	0.489	0.007	13.991	0.282	0.207	0.003	2563.927	30.449	2744.375	19.097	2880.943	20.339
137a-19	935.960	1028.930	1256.974	0.859	0.252	0.021	9.923	2.841	0.248	0.025	1398.507	56.911	2168.583	85.546	2962.440	80.828
137a-20	0.043	0.118	16192000.592	-3538.454124	4.34745E+14	8.45254E+13	5.91196E+16	1.14549E+16	0.991	0.006	193121.630	9071.838	35411.602	1428.499		
137a-21	423.291	439.504	2104.626	0.944	0.588	0.019	36.195	2.586	0.443	0.020	2968.963	75.707	3640.079	74.319	4023.255	67.570
137a-22	394.509	505.327	432.758	0.765	0.383	0.015	11.478	0.414	0.219	0.003	2081.654	71.542	2548.596	34.847	2971.296	23.696
137a-23	1638.316	9285.056	168186.452	0.171	4.672	1.768	603.362	234.745	0.884	0.028	6834.217	1542.691	5147.954	374.734	4854.386	34.053
137a-24	615.294	476.927	4262.739	1.243	0.541	0.119	36.445	14.975	0.376	0.049	2555.869	340.788	3183.787	247.014	3501.008	144.278
137a-25	2041.661	6024.308	25076.571	0.322	0.603	0.038	69.762	5.370	0.820	0.016	2997.139	148.443	4248.567	77.902	4828.031	34.255
137a-26	22.524	80.953	6635.338	-11384310.82	1.26979E+12	3.86772E+11	1.64307E+14	5.05283E+13	0.972	0.080	84987.579	17476.115	18226.168	2756.926	4713.088	71.994
137a-27	0.077	0.539	14.938	54712861.27	-3.71475E+11	95903335107	-5.19243E+13	1.5066E+13	1.113	0.199	25502.024	15469.984	6126.666	236.746	4448.563	135.752
137a-28	1286.113	5752.565	458.870	0.228	0.128	0.009	3.837	0.283	0.215	0.003	771.335	51.270	1554.065	58.945	2948.343	21.883
137a-29	957.973	3886.574	74098.439	0.428	3.280	0.855	421.130	118.196	0.789	0.060	7508.255	1149.464	5282.740	366.968	4185.681	305.585
137a-30	64.882	193.004	190.925	0.327	0.559	0.011	15.374	0.374	0.200	0.004	2859.933	46.998	2832.161	23.001	2814.106	32.237
137a-31	913.105	1592.774	4735.075	0.626	0.469	0.019	32.482	1.957	0.496	0.018	2464.328	85.757	3525.169	59.902	4200.562	54.139
137a-32	245.045	112.475	132.851	2.218	0.576	0.008	16.469	0.229	0.207	0.003	2930.017	33.532	2904.011	13.987	2877.187	21.506
137a-33	1467.782	3148.637	47402.633	0.466	1.089	0.185	128.672	24.196	0.754	0.030	4114.820	524.389	4363.831	211.733	4600.605	43.480
137a-34	916.465	5215.998	424.443	0.171	0.149	0.009	3.879	0.222	0.188	0.003	892.954	48.227	1589.458	46.575	2716.383	25.977
137a-35	134.295	98.822	123.720	1.298	0.570	0.014	15.421	0.585	0.198	0.006	2905.405	57.972	2837.025	36.761	2803.799	47.397
137a-36	873.715	5108.617	518.224	0.181	0.214	0.009	6.752	0.353	0.228	0.008	1245.506	47.199	2058.043	41.303	3015.777	44.192
137a-37	1254.407	4872.832	9147.742	0.252	0.416	0.018	38.701	2.752	0.648	0.019	2228.772	81.635	3694.941	68.323	4581.026	38.282
137a-38	1618.959	2538.050	3188.523	0.598	0.300	0.008	15.623	0.891	0.375	0.015	1695.874	39.379	2830.869	56.253	3782.630	60.348
137a-39	646.786	3499.931	10831.920	0.241	0.552	0.124	47.244	18.226	0.406	0.046	2474.864	367.521	3148.820	219.051	3503.650	69.462
137a-40	2267.995	11362.793	22313.580	0.187	0.445	0.027	49.280	3.223	0.792	0.010	2341.598	121.345	3910.425	72.054	4876.048	16.985
137a-41	516.832	413.289	524.017	1.208	0.348	0.009	10.094	0.238	0.208	0.003	1921.349	41.208	2440.398	21.851	2889.169	26.307
137a-42	2182.181	13985.691	60557.097	0.167	0.800	0.110	99.137	15.179	0.842	0.022	3493.841	354.442	4374.424	144.236	4805.240	35.717
137a-43	312.336	267.014	155.242	1.192	0.561	0.014	15.186	0.357	0.196	0.003	2863.142	56.055	2820.850	22.789	2792.274	21.665
137a-44	991.124	4241.609	67630.221	0.231	2.356	0.356	288.723	46.024	0.845	0.016	6888.598	627.404	5388.009	162.336	4863.044	22.950
137a-45	2188.697	1882.634	13663.675	1.157	0.344	0.034	31.647	4.182	0.618	0.021	1850.672	155.303	3349.816	115.669	4516.262	46.019

Grain	ppm U	Th	Pb	U/Th	Pb206/U238	2 SE	Pb207/U235	2 SE	Pb207/Pb206	2 SE	Age (Ma) Pb206/U238	2 SE	Age (Ma) Pb207/U235	2 SE	Age (Ma) Pb207/Pb206	2 SE
137-1	711.382	2325.186	365.705	0.290	0.184	0.005	4.764	0.132	0.187	0.003	1088.884	26.488	1772.228	23.012	2717.606	22.083
137-2	244.504	497.736	6507.306	0.479	1.509	0.068	144.767	7.336	0.695	0.014	5878.752	157.601	5030.399	46.237	4693.330	25.488
137-3	42.973	164.685	966.326	0.247	1.178	0.031	106.293	2.723	0.655	0.010	4998.925	89.418	4738.354	25.574	4628.228	22.100
137-4	1064.958	1638.354	2050.233	0.647	0.256	0.004	11.453	0.417	0.322	0.008	1470.951	21.166	2555.584	36.332	3569.571	41.335
137-5	851.953	3484.862	487.426	0.239	0.201	0.009	5.701	0.328	0.205	0.005	1177.544	47.363	1920.898	48.719	2856.218	35.069
137-6	1167.802	6552.851	796.893	0.198	0.161	0.011	4.195	0.285	0.190	0.003	952.609	59.797	1634.631	54.855	2737.409	26.611
137-7	0.000	0.000	-0.503	-9.81927E+21	-834260.9769	2278501.138	86293471.34	211089439.3	-0.650	3.227	92529.726	3558.363	20541.288	279.625	3328.038	433.261
137-8	15.831	35.488	239.672	0.576	1.099	0.052	78.544	3.761	0.522	0.015	4752.125	161.234	4421.811	49.047	4286.919	41.209
137-9	1.827	0.369	56.531	-1.9409E+31	385443.5997	764428.2048	456.9299152	110.290193	0.763	0.041	8541.546	802.262	5628.299	189.365	4580.248	53.574
137-10	1153.662	8332.247	19089.731	0.173	0.810	0.060	85.807	8.677	0.720	0.031	3798.711	225.917	4402.625	118.753	4618.999	92.626
137-11	965.209	4141.751	8233.478	0.227	0.471	0.043	46.105	5.811	0.672	0.028	2454.420	182.476	3831.893	128.963	4644.142	62.726
137-12	1807.825	8006.825	23918.534	0.218	0.557	0.087	60.480	10.936	0.717	0.024	2671.753	323.314	3835.780	162.487	4668.103	40.713
137-13	582.264	2852.161	596.020	0.217	0.318	0.010	8.517	0.428	0.191	0.004	1773.402	51.312	2261.565	44.133	2734.830	34.516
137-14	248.612	356.762	306.706	0.941	0.562	0.015	14.864	0.402	0.192	0.003	2865.430	60.555	2797.019	26.435	2749.638	21.996
137-15	285.050	282.515	187.935	1.003	0.454	0.007	12.366	0.224	0.198	0.003	2412.135	31.403	2630.779	17.424	2805.739	21.924
137-16	497.505	1337.285	319.548	0.387	0.334	0.014	8.668	0.389	0.185	0.003	1849.740	65.953	2279.897	43.618	2697.701	27.755
137-17	843.808	1809.344	408.968	0.451	0.268	0.005	7.066	0.224	0.191	0.004	1531.620	23.879	2111.002	24.621	2737.513	32.176
137-18	473.708	627.571	1739.109	0.918	0.463	0.058	24.011	11.288	0.283	0.022	2317.360	95.277	2845.388	59.776	3251.903	86.178
137-19	14.835	6.541	112.433	3.587	0.878	0.034	38.204	2.008	0.317	0.014	4040.656	118.694	3706.180	54.531	3525.303	66.601
137-20	951.924	9203.334	523.760	0.102	0.113	0.004	2.683	0.086	0.174	0.004	689.379	22.680	1319.738	24.138	2588.171	33.624
137-21	429.317	656.260	598.682	0.615	0.341	0.015	13.441	0.851	0.284	0.010	1887.790	71.103	2681.093	65.246	3365.934	60.240
137-22	144.156	106.802	61.324	1.333	0.602	0.011	16.693	0.356	0.200	0.003	3040.149	44.682	2911.636	20.118	2819.131	24.415
137-23	765.440	1677.703	2420.899	0.444	0.312	0.012	16.973	1.138	0.392	0.014	1742.283	55.241	2896.591	57.183	3851.622	48.277
137-24	1063.015	6890.849	22923.717	0.149	0.934	0.066	109.614	8.476	0.841	0.011	4183.062	211.607	4712.476	72.858	4919.942	14.345
137-25	10.937	48.405	314.818	0.220	1.358	0.060	110.645	4.384	0.602	0.014	5495.891	164.867	4771.923	41.442	4511.011	32.464
137-26	410.732	534.109	925.275	0.742	0.401	0.043	19.861	5.008	0.331	0.052	2161.076	195.242	2947.212	241.130	3519.861	238.624
137-27	269.682	393.455	192.138	0.686	0.410	0.009	11.357	0.232	0.200	0.003	2212.745	39.422	2548.244	19.061	2818.902	26.461
137-28	473.333	2838.481	356.831	0.159	0.255	0.005	6.554	0.127	0.186	0.002	1465.070	24.553	2049.128	17.193	2700.574	22.044
137-29	298.006	262.054	295.305	1.078	0.564	0.010	15.689	0.293	0.201	0.002	2880.748	41.431	2856.460	17.435	2831.663	17.982
137-30	375.358	416.547	193.094	0.858	0.486	0.015	13.523	0.412	0.202	0.003	2548.279	63.380	2707.671	29.386	2839.252	21.898
137-31	409.187	2502.951	284.870	0.160	0.199	0.004	5.216	0.119	0.190	0.003	1168.709	22.612	1850.373	19.451	2735.055	27.503
137-32	69.637	73772.867	66498.449	0.001	0.526	0.011	15.758	0.434	0.217	0.005	2720.818	45.997	2853.970	25.710	2944.143	36.816
137-33	284.145	492.509	143.943	0.564	0.481	0.008	13.132	0.246	0.197	0.003	2527.426	35.518	2685.174	17.826	2797.933	24.341
137-34	2326.769	12415.547	548242.808	0.176	8.891	1.162	1154.774	150.853	0.942	0.011	13707.862	692.685	6949.113	124.051	4919.738	41.496
137-35	0.004	0.291	2.869	-2.473E+45	671087.6565	270988.4245	92896118.72	22167805.82	0.983	0.891	84421.035	2351.290	18856.933	178.790	3708.432	338.600
137-36	388.461	226.330	128.708	1.821	0.496	0.007	13.674	0.214	0.199	0.002	2593.489	31.949	2724.359	14.860	2816.096	18.311
137-37	326.725	1098.585	1385.730	0.282	0.554	0.020	31.014	1.545	0.399	0.010	2837.471	82.537	3506.296	47.236	3899.759	35.995
137-38	0.457	0.868	220.577	2.63522E+53	-408042735.7	228818292.2	-56450163031	31494812975	1.033	0.028	20170.126	1000.516	8143.924	169.035	4926.864	59.800
137-39	885.820	1927.694	22353.519	0.442	1.294	0.140	150.882	18.630	0.810	0.018	5044.826	359.606	4895.713	119.130	4814.333	32.708
137-40	56.950	182.594	81.184	0.320	0.513	0.015	14.434	0.413	0.204	0.005	2663.305	62.834	2773.705	28.725	2844.001	38.144
137-41	1389.950	5940.518	269028.715	0.229	8.446	1.045	1105.341	126.662	0.971	0.016	14083.870	637.613	7057.524	111.336	4933.253	30.358
137-42	0.032	0.310	2.148	8.65685E+54	-24139948491	7687733931	-2.68739E+12	7.64346E+11	0.717	0.421	87851.080	22140.592	15923.156	4192.358	3707.821	294.962
137-43	0.017	0.335	2.858	-5.86476E+55	81689836867	25128969745	7.69471E+12	2.15734E+12	1.006	0.457	133618.284	12426.886	26055.602	1971.501	3664.015	323.658
137-44	299.765	314.556	179.762	0.936	0.440	0.017	12.295	0.473	0.203	0.004	2342.779	75.071	2615.048	36.303	2846.481	27.949
137-45	458.161	1444.450	419.130	0.309	0.293	0.008	8.039	0.243	0.197	0.003	1661.451	36.983	2225.259	28.058	2793.602	24.612
137-46	458.107	1495.940	367.635	0.317	0.398	0.008	10.764	0.234	0.196	0.002	2157.000	35.363	2500.302	20.558	2785.744	20.775
137-47	653.605	1823.198	337.318	0.566	0.294	0.016	8.286	0.442	0.203	0.003	1646.357	79.533	2228.123	52.507	2849.133	21.547
137-48	924.997	7429.136	435.200	0.120	0.118	0.004	3.138	0.110	0.192	0.003	720.736	20.767	1432.510	26.289	2747.587	29.063
137-49	14.577	46.612	323.713	0.297	1.328	0.051	123.823	4.455	0.668	0.016	5428.447	144.723	4883.448	36.230	4638.243	33.136
137-50	2492.723	11203.519	22656.429	0.214	0.475	0.074	56.571	9.352	0.842	0.015	2348.791	280.087	3890.614	128.197	4891.322	22.469
137-51	599.951	1178.954	440.869	0.842	0.410	0.017	11.802	0.477	0.208	0.003	2199.723	78.357	2569.250	37.181	2884.579	20.922
137-52	800.449	2302.503	988.623	0.318	0.340	0.022	11.806	1.648	0.247	0.019	1864.746	104.108	2513.823	115.242	3091.722	96.799
137-53	177.790	96.565	48.188	2.343	0.569	0.014	15.192	0.403	0.193	0.003	2898.663	56.129	2820.647	25.612	2768.291	30.414
137-54	290.381	208.907	158.027	1.538	0.566	0.011	16.640	0.356	0.212	0.003	2887.267	47.113	2909.872	20.294	2923.273	22.294
137-55	247.163	208.876	246.296	1.128	0.579	0.012	17.185	0.324	0.213	0.003	2946.632	51.400	2940.944	18.180	2923.692	24.871
137-56	467.831	503.407	270.882	0.886	0.494	0.012	13.980	0.362	0.203	0.003	2581.407	50.751	2744.026	24.313	2848.882	22.603

Appendix 3

Table 4. Analyses from sample LST12-138.7.

Grains	ppm U	Th	Pb	U/Th	Pb206/U238	2 SE	Pb207/U235	2 SE	Pb207/Pb206	2 SE	Age (Ma) Pb206/U238	2 SE	Age (Ma) Pb207/U235	2 SE	Age (Ma) Pb207/Pb206	2 SE
138.7-1	657.514	512.153	918.843	1.238	0.399	0.009	14.156	0.484	0.250	0.005	2164.425	40.405	2751.502	33.730	3179.062	29.915
138.7-2	1153.630	3743.959	5588.949	0.306	0.337	0.014	28.702	1.830	0.587	0.018	1869.473	65.169	3424.218	60.192	4466.728	44.847
138.7-3	3295.298	12136.463	334055.066	0.258	3.948	0.554	485.613	65.195	0.923	0.017	9587.215	627.787	6132.952	120.819	4694.148	100.301
138.7-4	685.107	1245.826	357.080	0.520	0.320	0.013	8.468	0.403	0.187	0.003	1782.040	63.665	2259.869	43.034	2712.023	27.883
138.7-5	1296.828	1911.072	14091.023	0.663	0.607	0.094	58.956	11.685	0.614	0.037	2964.918	346.430	3857.286	195.284	4379.551	100.487
138.7-6	1838.666	7432.516	200786.143	0.247	3.886	0.859	509.893	116.485	0.839	0.031	7949.086	1070.993	5472.405	297.988	4598.326	87.041
138.7-7	857.681	2336.954	1088.472	0.368	0.346	0.007	12.359	0.255	0.251	0.004	1913.568	33.017	2628.541	19.444	3188.319	25.484
138.7-9	135.662	95.467	191.212	1.368	0.596	0.011	20.336	0.911	0.243	0.008	3017.301	45.860	3092.351	41.599	3117.110	50.740
138.7-10	106.564	68.577	58.734	1.718	0.543	0.015	15.607	0.451	0.206	0.003	2786.729	62.933	2843.459	28.266	2874.822	29.260
138.7-11	2084.219	2686.889	83422.307	0.765	1.348	0.242	168.650	32.704	0.787	0.036	4745.156	612.087	4614.498	241.608	4542.836	80.547
138.7-12	681.511	1802.348	16154.820	0.375	0.909	0.176	94.048	22.692	0.661	0.041	3718.197	442.286	4249.197	208.430	4417.065	88.946
138.7-13	464.107	589.687	6625.742	0.785	0.932	0.043	85.328	6.071	0.636	0.018	4206.764	140.473	4475.593	72.486	4583.101	39.666
138.7-14	2519.288	5572.698	33250.862	0.422	0.536	0.074	65.278	9.672	0.857	0.024	2720.467	310.013	4091.984	160.428	4850.973	38.441
138.7-15	868.822	1152.164	989.804	0.960	0.294	0.007	11.907	0.430	0.292	0.007	1661.102	35.731	2588.357	34.336	3416.125	36.161
138.7-16	391.641	629.968	1103.726	1.210	0.557	0.044	23.671	6.484	0.287	0.034	2809.763	139.473	3022.611	100.380	3095.350	72.912
138.7-17	1546.479	6913.591	111320.028	0.247	1.912	0.495	225.918	61.070	0.812	0.021	6069.179	805.770	5097.806	201.378	4807.777	37.759
138.7-18	1500.558	24303.074	361.747	0.070	0.024	0.002	0.565	0.039	0.172	0.007	154.626	9.600	451.130	24.721	2531.265	70.271
138.7-19	1208.958	2642.518	60203.714	0.442	1.855	0.201	229.712	27.640	0.857	0.018	6457.669	435.245	5347.751	122.705	4884.248	26.092
138.7-20	507.881	418.296	4367.389	1.282	0.642	0.103	48.357	15.019	0.410	0.038	3116.944	342.757	3549.897	191.521	3744.966	103.504
138.7-21	1355.611	13284.283	177640.456	0.104	3.936	1.456	486.866	182.839	0.769	0.027	5616.542	1353.651	4534.490	355.915	4723.474	41.893
138.7-22	547.700	828.273	573.444	0.668	0.366	0.009	11.029	0.276	0.218	0.003	2005.823	42.579	2518.876	23.537	2962.638	23.765
138.7-23	1405.460	5348.828	178096.277	0.263	4.075	0.846	526.433	112.380	0.886	0.019	8718.197	969.588	5800.620	232.198	4871.007	39.632
138.7-26	1390.060	1636.432	2515.509	0.870	0.260	0.028	13.794	2.415	0.382	0.023	1481.289	141.527	2688.973	149.800	3786.781	71.785
138.7-27	419.025	337.037	471.067	1.176	0.522	0.012	14.367	0.348	0.198	0.003	2701.220	48.782	2767.729	23.177	2801.991	27.474
138.7-28	1705.066	7378.975	5129.122	0.241	0.215	0.013	16.168	1.166	0.538	0.016	1244.890	69.249	2832.769	65.719	4330.105	43.472
138.7-29	1046.723	593.716	760.534	1.649	0.255	0.004	7.250	0.187	0.203	0.003	1464.637	20.700	2136.156	23.178	2843.551	24.576
138.7-30	587.745	153.517	1563.258	3.850	0.635	0.014	26.687	1.241	0.305	0.012	3182.522	60.275	3372.622	46.503	3476.926	56.345
138.7-31	1863.268	8457.562	648.647	0.216	0.119	0.005	2.959	0.137	0.178	0.002	721.754	31.039	1382.318	34.945	2631.354	22.444
138.7-32	1133.793	3263.637	14359.943	0.325	0.714	0.194	62.699	25.542	0.326	0.050	2829.935	512.523	2937.861	264.804	3008.374	102.754
138.7-33	455.027	1447.415	762.249	0.292	0.330	0.009	9.335	0.304	0.201	0.003	1836.297	42.423	2365.089	29.062	2828.888	25.380
138.7-34	2283.400	6357.483	43867.010	0.341	0.790	0.090	99.527	12.678	0.847	0.021	3600.421	329.257	4453.132	143.130	4846.068	31.378
138.7-35	370.289	1319.804	2220.821	0.261	0.609	0.009	17.382	0.262	0.204	0.003	3064.355	36.706	2953.577	14.554	2856.676	21.254
138.7-36	333.861	317.574	542.368	0.976	0.583	0.010	17.057	0.265	0.209	0.003	2959.445	39.082	2935.293	15.093	2896.620	24.201

	ppm										Age (Ma)		Age (Ma)		Age (Ma)	
Grains	U	Th	Pb	U/Th	Pb206/U238	2 SE	Pb207/U235	2 SE	Pb207/Pb206	2 SE	Pb206/U238	2 SE	Pb207/U235	2 SE	Pb207/Pb206	2 SE
138.7-37	1965.385	3640.843	55415.831	0.536	1.360	0.217	167.140	28.686	0.843	0.017	4979.460	510.309	4878.989	158.846	4863.471	26.538
138.7-38	204.333	238.357	225.642	1.044	0.559	0.009	15.608	0.303	0.203	0.003	2861.091	37.063	2849.717	18.428	2842.709	26.417
138.7-39	134.447	163.627	153.508	0.750	0.509	0.012	13.875	0.412	0.199	0.004	2648.026	52.864	2738.588	28.335	2802.802	34.293
138.7-40	1039.236	4194.833	17736.041	0.263	0.769	0.086	88.090	11.197	0.791	0.025	3530.881	283.207	4372.815	118.208	4743.088	49.489
138.7-41	563.631	927.958	739.909	0.577	0.290	0.008	10.742	0.419	0.272	0.008	1637.072	38.862	2487.277	31.442	3301.614	41.964
138.7-42	777.164	2849.387	328.076	0.299	0.193	0.016	5.064	0.459	0.189	0.003	1121.375	85.586	1766.160	75.592	2725.681	27.641
138.7-43	197.830	384.367	324.820	0.505	0.436	0.010	12.619	0.318	0.209	0.004	2326.779	46.502	2644.348	23.390	2888.847	31.461
138.7-44	2195.144	7242.461	214722.523	0.293	3.400	0.596	438.926	75.994	0.951	0.012	8434.557	719.681	5884.238	156.887	4974.971	27.046
138.7-45	357.567	1663.275	244.309	0.207	0.255	0.008	7.199	0.232	0.204	0.004	1458.711	39.587	2124.743	29.553	2851.703	28.514
138.7-46	749.000	2913.253	518.712	0.246	0.236	0.011	7.708	0.477	0.232	0.006	1361.064	57.706	2155.994	59.529	3049.182	39.757
138.7-47	305.980	534.968	329.345	0.606	0.381	0.015	11.503	0.440	0.218	0.004	2071.798	68.524	2546.825	35.977	2962.580	27.777
138.7-48	0.000	0.057	2.780	-1539.30119	2125771.092	496013.6916	256754127.2	47415230.65	-5.511	2.866	95791.126	1067.497	19707.240	162.620	3830.371	236.836
138.7-49	924.738	4172.554	2246.523	0.211	0.255	0.010	15.843	0.847	0.441	0.013	1456.885	50.212	2827.863	54.342	4036.882	42.875
138.7-50	1013.051	2955.713	8926.185	0.324	0.462	0.032	48.166	4.411	0.708	0.025	2420.531	145.955	3812.143	106.757	4649.739	56.246
138.7-51	0.068	0.195	5.198	2859056.152	-118757395	41999094.56	-1.334E+10	4174756454	-0.870	1.360	29940.492	12857.186	6681.226	2149.879	3945.968	228.097
138.7-52	1271.174	4062.680	67931.801	0.300	2.275	0.235	295.641	31.272	0.913	0.014	7328.066	454.968	5640.849	109.414	4927.961	26.294
138.7-53	1507.629	4293.431	7607.450	0.339	0.325	0.014	28.813	1.941	0.626	0.017	1805.947	65.485	3407.932	60.438	4530.882	32.938
138.7-54	875.602	1618.781	916.895	0.569	0.330	0.011	10.823	0.292	0.240	0.006	1833.234	55.095	2502.094	25.286	3107.726	37.145
138.7-55	454.613	509.822	279.539	0.877	0.371	0.008	10.825	0.283	0.209	0.003	2033.194	37.902	2503.353	23.849	2901.692	24.627
138.7-56	1413.836	7570.069	368.437	0.181	0.085	0.005	2.306	0.138	0.195	0.003	522.708	27.114	1195.712	43.493	2776.221	26.445
138.7-57	646.779	1934.780	376.707	0.339	0.275	0.007	7.499	0.217	0.196	0.003	1564.298	33.326	2163.696	26.398	2789.945	21.495
138.7-58	1717.021	4033.035	230044.359	0.401	6.234	0.768	827.877	103.150	0.940	0.014	11940.229	784.435	6619.154	158.408	4898.807	48.271
138.7-59	204.457	552.674	192.739	0.361	0.424	0.013	11.268	0.340	0.191	0.003	2271.228	56.532	2534.042	28.564	2745.923	28.578
138.7-60	1166.996	4031.675	36137.378	0.277	1.472	0.301	200.441	44.772	0.902	0.017	5386.403	659.043	4994.708	182.284	4826.242	78.956
138.7-61	192.189	194.287	214.390	0.972	0.558	0.011	15.825	0.319	0.205	0.003	2854.718	43.688	2864.158	19.504	2859.057	24.942
138.7-62	1306.749	5252.112	18573.998	0.270	0.801	0.104	95.076	13.948	0.701	0.050	3467.177	375.692	4018.480	248.249	4203.447	198.430
138.7-63	489.702	1411.292	624.353	0.354	0.286	0.010	7.714	0.294	0.194	0.003	1620.252	53.383	2186.151	33.632	2771.110	24.534
138.7-64	1389.537	4287.883	98509.671	0.316	2.911	0.306	390.822	43.444	0.933	0.012	8636.696	602.236	5939.900	130.672	4859.537	104.227
138.7-65	427.214	551.902	766.270	0.757	0.566	0.013	16.247	0.350	0.206	0.002	2890.823	54.689	2885.300	20.683	2869.971	16.715
138.7-66	171.637	99.328	457.708	1.736	0.650	0.014	26.714	1.130	0.294	0.009	3222.308	52.547	3353.676	42.126	3416.564	48.305

References

Albani, A. El, Bengtson, S., Canfield, D. E., Bekker, A., MacChiarelli, R., Mazurier, A., Hammarlund, E. U., Boulvais, P., Dupuy, J. J., Fontaine, C., Fürsich, F. T., Gauthier-Lafaye, F., Janvier, P., Javaux, E., Ossa, F. O., Pierson-Wickmann, A. C., Riboulleau, A., Sardini, P., Vachard, D., Meunier, A. (2010). Large colonial organisms with coordinated growth in oxygenated environments 2.1 Gyr ago. *Nature*, *466*(7302), 100–104. https://doi.org/10.1038/nature09166

Ausmeel, M. (2020). Lewisian'i gneisikompleksi tsirkooni megakristallide sobivuse hindamine in-house U - Pb dateerimise standardina LA-ICP-MS meetodil.

Bankole, O. M., El Albani, A., Meunier, A., Pambo, F., Paquette, J. L., & Bekker, A. (2018). Earth's oldest preserved K-bentonites in the CA. 2.1 Ga Francevillian Basin, Gabon. *American Journal of Science*, *318*(4), 409–434. https://doi.org/10.2475/04.2018.02

Barbeau, D. L., Olivero, E. B., Swanson-Hysell, N. L., Zahid, K. M., Murray, K. E., & Gehrels, G. E. (2009). Detrital-zircon geochronology of the eastern Magallanes foreland basin: Implications for Eocene kinematics of the northern Scotia Arc and Drake Passage. *Earth and Planetary Science Letters*, *284*(3–4), 489–503. https://doi.org/10.1016/j.epsl.2009.05.014

Barham, M., Kirkland, C. L., Hovikoski, J., Alsen, P., Hollis, J., & Tyrrell, S. (2021). Reduce or recycle? Revealing source to sink links through integrated zircon–feldspar provenance fingerprinting. *Sedimentology*, *68*(2), 531–556. https://doi.org/10.1111/sed.12790

Blättler, C. L., Claire, M. W., Prave, A. R., Kirsimäe, K., Higgins, J. A., Medvedev, P. V, Romashkin, A. E., Rychanchik, D. V, Zerkle, A. L., Paiste, K., Kreitsmann, T., Millar, I. L., Hayles, J. A., Bao, H., Turchyn, A. V, Warke, M. R., & Lepland, A. (2018). Two-billion-year-old evaporites capture Earth's great oxidation. In *Science* (Vol. 360). https://www.science.org

Bonhomme, M. G., Gauthier-Lafaye, F., & Weber, F. (1982). An example of lower proterozoic sediments: The Francevillian in Gabon. *Precambrian Research*, *18*(1–2), 87–102. https://doi.org/10.1016/0301-9268(82)90038-9

Bowring, S. A., Schoene, B., Crowley, J. L., Ramezani, J., & Condon, D. J. (2006). High-Precision U-Pb Zircon Geochronology and the Stratigraphic Record: Progress and Promise. *The Paleontological Society Papers*, *12*, 25–45. https://doi.org/10.1017/S1089332600001339

Bros, R., Stille, P., Gauthier-Lafaye, F., Weber, F., & Clauer, N. (1992). Sm-Nd isotopic dating of Proterozoic clay material: An example from the Francevillian sedimentary series, Gabon. *Earth and Planetary Science Letters*, *113*(1–2), 207–218. https://doi.org/10.1016/0012-821X(92)90220-P

Cawood, P. A., & Nemchin, A. A. (2000). Provenance record of a rift basin: U/Pb ages of detrital zircons from the Perth Basin, Western Australia. *Sedimentary Geology*, *134*(3–4), 209–234. https://doi.org/10.1016/S0037-0738(00)00044-0

Dröllner, M., Barham, M., Kirkland, C. L., & Ware, B. (2021). Every zircon deserves a date: Selection bias in detrital geochronology. *Geological Magazine*, *158*(6), 1135–1142. https://doi.org/10.1017/S0016756821000145

Eyster, A., Tappa, M. J., Abdul Rashid, S., Lepland, A., Rooney, A. D., & Bauer, A. (2022). Evaluating basinal and global repercussions of the initial rise of oxygen via geochemical

constraints from the Paleoproterozoic Onega Basin, Fennoscandian Shield. *AGU Fall Meeting*, 52B – 05.

Faithfull, J. W., Dempster, T. J., MacDonald, J. M., & Reilly, M. (2018). Metasomatism and the crystallization of zircon megacrysts in Archaean peridotites from the Lewisian complex, NW Scotland. *Contributions to Mineralogy and Petrology*, *173*(12). https://doi.org/10.1007/s00410-018-1527-5

Farquhar, J., Bao, H., & Thiemens, M. (2000). Atmospheric influence of Earth's earliest sulfur cycle. *Science*, *289*, 756–758.

Fedo, C. M., Sircombe, K. N., & Rainbird, R. H. (2003). Detrital zircon analysis of the sedimentary record. *Reviews in Mineralogy and Geochemistry*, *53*. https://doi.org/10.2113/0530277

Gauthier-Lafaye, F., & Weber, F. (1989). The Francevillian (Lower Proterozoic) Uranium Ore-Deposits of Gabon. *Economic Geology*, *84*(8), 2267–2285. http://pubs.geoscienceworld.org/segweb/economicgeology/article-pdf/84/8/2267/3490421/2267.pdf

Gauthier-Lafaye, F., & Weber, F. (2003). Natural nuclear fission reactors: time constraints for occurrence, and their relation to uranium and manganese deposits and to the evolution of the atmosphere. *Precrambian Research*, *120*, 81–100. www.elsevier.com/locate/precamres

Gehrels, G. (2011). Detrital Zircon U-Pb Geochronology: Current Methods and New Opportunities. In *Tectonics of Sedimentary Basins* (pp. 45–62). Wiley. https://doi.org/10.1002/9781444347166.ch2

Gehrels, G. (2014). Detrital zircon U-Pb geochronology applied to tectonics. In *Annual Review of Earth and Planetary Sciences* (Vol. 42, pp. 127–149). Annual Reviews Inc. https://doi.org/10.1146/annurev-earth-050212-124012

Gehrels, G. E. (2000). Introduction to detrital zircon studies of Paleozoic and Triassic strata in western Nevada and northern California. In *Paleozoic and Triassic paleogeography and tectonics of western Nevada and Northern California*. Geological Society of America. https://doi.org/10.1130/0-8137-2347-7.1

Gumsley, A. P., Chamberlain, K. R., Bleeker, W., Söderlund, U., De Kock, M. O., Larsson, E. R., & Bekker, A. (2017). Timing and tempo of the great oxidation event. *Proceedings of the National Academy of Sciences of the United States of America*, *114*(8), 1811–1816. https://doi.org/10.1073/pnas.1608824114

Hietpas, J., Samson, S., & Moecher, D. (2011). A direct comparison of the ages of detrital monazite versus detrital zircon in Appalachian foreland basin sandstones: Searching for the record of Phanerozoic orogenic events. *Earth and Planetary Science Letters*, *310*(3–4), 488–497. https://doi.org/10.1016/J.EPSL.2011.08.033

Hilbert-Wolf, H., Roberts, E., Downie, B., Mtelela, C., Stevens, N. J., & O'Connor, P. (2017). Application of U–Pb detrital zircon geochronology to drill cuttings for age control in hydrocarbon exploration wells: A case study from the Rukwa Rift Basin, Tanzania. *AAPG Bulletin*, *101*(02), 143–159. https://doi.org/10.1306/06281616003

Hodgskiss, M. S. W., Crockford, P. W., & Turchyn, A. V. (2023). Deconstructing the Lomagundi-Jatuli Carbon Isotope Excursion. https://doi.org/10.1146/annurev-earth-031621

Holland, H. D. (2006). The oxygenation of the atmosphere and oceans. *Philosophical Transactions of the Royal Society B: Biological Sciences*, *361*(1470), 903–915. https://doi.org/10.1098/rstb.2006.1838

Horie, K., Hidaka, H., & Gauthier-Lafaye, F. (2005). U-Pb geochronology and geochemistry of zircon from the Franceville series at Bidoudouma, Gabon. In *Geochimia et Cosmochimica Acta* (Vol. 69, Issue 10, pp. A11–A11).

Juhkama, H.-R. (2020). Mn-carbonates in carbonate-shale succession in Palaeoproterozoic Lastoursville sub-basin, Gabon.

Karhu, J. A., & Holland, H. D. (1996). Carbon isotopes and the rise of atmospheric oxygen. *Geology*, *24*(10), 867–870. http://pubs.geoscienceworld.org/gsa/geology/article-pdf/24/10/867/3515968/i0091-7613-24-10-867.pdf

Kuusk, C. (2021). Dating zircons from Francevillian Basin by laser-ablation inductively coupled plasma mass-spectrometry.

Lepland, A., Melezhik, V. A., Papineau, D., Romashkin, A. E., & Joosu, L. (2013). 7.7 The Earliest Phosphorites: Radical Change in the Phosphorus Cycle During the Palaeoproterozoic. *Frontiers in Earth Sciences*, *8*, 1275–1296. https://doi.org/10.1007/978-3-642-29670-3_7

Luo, G., Ono, S., Beukes, N. J., Wang, D. T., Xie, S., & Summons, R. E. (2016). Rapid oxygenation of Earth's atmosphere 2.33 billion years ago. *Science Advances*, *2*(5). https://doi.org/10.1126/SCIADV.1600134

Lyons, T. W., Reinhard, C. T., & Planavsky, N. J. (2014). The rise of oxygen in Earth's early ocean and atmosphere. In *Nature* (Vol. 506, Issue 7488, pp. 307–315). Nature Publishing Group. https://doi.org/10.1038/nature13068

Macdonald, J. D., Holford, S. P., Green, P. F., Duddy, I. R., King, R. C., & Backé, G. (2013). Detrital zircon data reveal the origin of Australia's largest delta system. *Journal of the Geological Society*, *170*, 3–6. https://doi.org/10.1144/jgs2012-093

Malusà, M. G., Resentini, A., & Garzanti, E. (2016). Hydraulic sorting and mineral fertility bias in detrital geochronology. *Gondwana Research*, *31*, 1–19. https://doi.org/10.1016/J.GR.2015.09.002

Martin, A. P., Condon, D. J., Prave, A. R., & Lepland, A. (2013). A review of temporal constraints for the Palaeoproterozoic large, positive carbonate carbon isotope excursion (the Lomagundi–Jatuli Event). *Earth-Science Reviews*, *127*, 242–261. https://doi.org/10.1016/J.EARSCIREV.2013.10.006

Mathieu, R., Cuney, M., & Cathelineau, M. (2000). Geochemistry of palaeofluids circulation in the Franceville basin and around Oklo natural nuclear reaction zones (Gabon). *Journal of Geochemical Exploration*, *69–70*, 245–249. https://doi.org/10.1016/S0375-6742(00)00054-6

Mathieu, R., Zetterström, L., Cuney, M., Gauthier-Lafaye, F., & Hidaka, H. (2001). Alteration of monazite and zircon and lead migration as geochemical tracers of fluid paleocirculations around the Oklo–Okelobondo and Bangombe natural nuclear reaction zones (Franceville basin, Gabon). *Chemical Geology*, *171*, 147–171.

Mayika, K. B., Moussavou, M., Prave, A. R., Lepland, A., Mbina, M., & Kirsimäe, K. (2020). The Paleoproterozoic Francevillian succession of Gabon and the Lomagundi-Jatuli event. *Geology*, *48*(11), 1099–1104. https://doi.org/10.1130/g47651.1

Melezhik, V. A., Fallick, A. E., Filippov, M. M., Deines, Y. E., Črne, A. E., Lepland, A., Brasier, A. T., & Strauss, H. (2012). Giant Palaeoproterozoic Petrified Oil Field in the Onega Basin. In V. A. Melezhik, A. R. Prave, A. E. Fallick, L. R. Kump, H. Strauss, A. Lepland, & E. J. Hanski (Eds.), Reading the Archive of Earth's Oxygenation: Volume 3: Global Events and the Fennoscandian Arctic Russia - Drilling Early Earth Project (pp. 1202–1212). Frontiers in Earth Sciences. Springer.

Moecher, D. P., & Samson, S. D. (2006). Differential zircon fertility of source terranes and natural bias in the detrital zircon record: Implications for sedimentary provenance analysis. *Earth and Planetary Science Letters*, *247*(3–4), 252–266. https://doi.org/10.1016/J.EPSL.2006.04.035

Mouélé, I. M., Dudoignon, P., El Albani, A., Meunier, A., Boulvais, P., Gauthier-Lafaye, F., Paquette, J. L., Martin, H., & Cuney, M. (2014). 2.9-1.9Ga paleoalterations of Archean granitic basement of the Franceville basin (Gabon). *Journal of African Earth Sciences*, *97*, 244–260. https://doi.org/10.1016/j.jafrearsci.2014.04.027

Moussavou, M., & Minko, A. E. (2006). Contribution a l'histoire thermo-tectonique precambrienne du complexe annulaire de N'goutou par la geochimie et la geochronologie U/Pb sur mineraux accessoires (Bassin Francevillien d'Okondja, Gabon). *Africa Geoscience Review*, *13*(1/2), 53.

Nelson, D. R. (2001). An assessment of the determination of depositional ages for precambrian clastic sedimentary rocks by U–Pb dating of detrital zircons. *Sedimentary Geology*, *141–142*, 37–60. https://doi.org/10.1016/S0037-0738(01)00067-7

Ossa Ossa, F., Eickmann, B., Hofmann, A., Planavsky, N. J., Asael, D., Pambo, F., & Bekker, A. (2018). Two-step deoxygenation at the end of the Paleoproterozoic Lomagundi Event. *Earth and Planetary Science Letters*, *486*, 70–83. https://doi.org/10.1016/j.epsl.2018.01.009

Ossa Ossa, F., El Albani, A., Hofmann, A., Bekker, A., Gauthier-Lafaye, F., Pambo, F., Meunier, A., Fontaine, C., Boulvais, P., Pierson-Wickmann, A. C., Cavalazzi, B., & Macchiarelli, R. (2013). Exceptional preservation of expandable clay minerals in the ca. 2.1Ga black shales of the Francevillian basin, Gabon, and its implication for atmospheric oxygen accumulation. *Chemical Geology*, *362*, 181–192. https://doi.org/10.1016/j.chemgeo.2013.08.011

Ossa Ossa, F., Hofmann, A., Ballouard, C., Voster, C., Schoenberg, R., Fiedrich, A., Mayaga-Mikolo, F., & Bekker, A. (2020). Constraining provenance for the uraniferous Paleoproterozoic Francevillian Group sediments (Gabon) with detrital zircon geochronology and geochemistry. *Precambrian Research*, *343*. https://doi.org/10.1016/j.precamres.2020.105724

Ossa Ossa, F., Hofmann, A., Vidal, O., Kramers, J. D., Agangi, A., Belyanin, G. A., & Mayaga-Mikolo, F. (2014). Hydrothermal clay mineral formation in the uraniferous Paleoproterozoic FA Formation, Francevillian basin, Gabon. *Precambrian Research*, *246*, 134–149. https://doi.org/10.1016/j.precamres.2014.03.003

Paiste, K., Fike, D. A., Mayika, K. B., Moussavou, M., Lepland, A., Prave, A. R., Sato, T., Ueno, Y., Sawaki, Y., Richardson, J. A., Wood, R. S., Jones, C., Webb, S. M., & Kirsimäe, K. (2024). Sulfur isotopes from the Paleoproterozoic Francevillian Basin record multiple mineralizing events disallowing reconstruction of depositional conditions. *Nature Communications Earth & Environment*, in Press.

Poulton, S. W., Bekker, A., Cumming, V. M., Zerkle, A. L., Canfield, D. E., & Johnston, D. T. (2021). A 200-million-year delay in permanent atmospheric oxygenation. *Nature*, *592*(7853), 232–236. https://doi.org/10.1038/s41586-021-03393-7

Prave, A. R., Kirsimäe, K., Lepland, A., Fallick, A. E., Kreitsmann, T., Deines, Yu. E., Romashkin, A. E., Rychanchik, D. V., Medvedev, P. V., Moussavou, M., Bakakas, K., & Hodgskiss, M. S. W. (2022). The grandest of them all: the Lomagundi–Jatuli Event and Earth's oxygenation. *Journal of the Geological Society*, *179*(1). https://doi.org/10.1144/jgs2021-036

Préat, A., Bouton, P., Thiéblemont, D., Prian, J. P., Ndounze, S. S., & Delpomdor, F. (2011). Paleoproterozoic high δ13C dolomites from the Lastoursville and Franceville basins (SE Gabon): Stratigraphic and synsedimentary subsidence implications. *Precambrian Research*, *189*(1–2), 212–228. https://doi.org/10.1016/j.precamres.2011.05.013

Roberts, N. M. W., Drost, K., Horstwood, M. S. A., Condon, D. J., Chew, D., Drake, H., Milodowski, A. E., McLean, N. M., Smye, A. J., Walker, R. J., Haslam, R., Hodson, K., Imber, J., Beaudoin, N., & Lee, J. K. (2020). Laser ablation inductively coupled plasma mass spectrometry (LA-ICP-MS) U–Pb carbonate geochronology: strategies, progress, and limitations. *Geochronology*, *2*(1), 33–61. https://doi.org/10.5194/gchron-2-33-2020

Sawaki, Y., Moussavou, M., Sato, T., Suzuki, K., Ligna, C., Asanuma, H., Sakata, S., Obayashi, H., Hirata, T., & Edou-Minko, A. (2017). Chronological constraints on the Paleoproterozoic Francevillian Group in Gabon. *Geoscience Frontiers*, *8*(2), 397–407. https://doi.org/10.1016/J.GSF.2016.10.001

Sharman, G. R., & Malkowski, M. A. (2020). Needles in a haystack: Detrital zircon UPb ages and the maximum depositional age of modern global sediment. *Earth-Science Reviews*, *203*, 103109. https://doi.org/10.1016/J.EARSCIREV.2020.103109

Sircombe, K. N., & Stern, R. A. (2002). An investigation of artificial biasing in detrital zircon U-Pb geochronology due to magnetic separation in sample preparation. *Geochimica et Cosmochimica Acta*, *66*(13), 2379–2397. https://doi.org/10.1016/S0016-7037(02)00839-6

Sláma, J., & Košler, J. (2012). Effects of sampling and mineral separation on accuracy of detrital zircon studies. *Geochemistry, Geophysics, Geosystems*, *13*(5). https://doi.org/10.1029/2012GC004106

Spencer, C. J., Kirkland, C. L., & Roberts, N. M. W. (2018). Implications of erosion and bedrock composition on zircon fertility: Examples from South America and Western Australia. *Terra Nova*, *30*(4), 289–295. https://doi.org/10.1111/ter.12338

Stille, P., Gauthier-Lafaye, F., & Bros, R. (1993). The neodymium isotope system as a tool for petroleum exploration. *Geochimica et Cosmochimica Acta*, *57*(18), 4521–4525. https://doi.org/10.1016/0016-7037(93)90502-N

Thiéblemont, D., Bouton, P., Préat, A., Goujou, J. C., Tegyey, M., Weber, F., Obiang, M. E., Joron, J. L., & Treuil, M. (2014). Transition from alkaline to calc-alkaline volcanism during evolution of the Paleoproterozoic Francevillian basin of eastern Gabon (Western Central Africa). *Journal of African Earth Sciences*, *99*(PA2), 215–227. https://doi.org/10.1016/J.JAFREARSCI.2013.12.007

Thiéblemont, P., Castaing, C., Billa, M., Bouton, P., & Préat, A. (2009). *Notice explicative de la carte géologique et des ressources minérales de la République Gabonaise à 1/1000 000:* Libreville, Gabon, Ministère des Mines, du Pétrole, des Hydrocarbures, Libreville.

Vermeesch, P. (2021). On the treatment of discordant detrital zircon U–Pb data. *Geochronology*, *3*(1), 247–257. https://doi.org/10.5194/gchron-3-247-2021

Villa, I. M., & Hanchar, J. M. (2017). Age discordance and mineralogy. *American Mineralogist*, *102*(12), 2422–2439. https://doi.org/10.2138/am-2017-6084

Weber, F. (1968). Une série précambrienne du Gabon: le Francevillien Sédimentologie, géochimie, relations avec les gîtes minéraux associés. [CEA-R-40055]. Université de Strasbourg, Strasbourg.

Weber, F., & Gauthier-Lafaye, F. (2013). No proof from carbon isotopes in the Francevillian (Gabon) and Onega (Fennoscandian shield) basins of a global oxidation event at 1980–

2090 Ma following the Great Oxidation Event (GOE). *Comptes Rendus. Géoscience, 345*(1), 28–35. https://doi.org/10.1016/j.crte.2012.12.003

Weber, F., Gauthier-Lafaye, F., Whitechurch, H., Ulrich, M., & El Albani, A. (2016). The 2-Ga Eburnean Orogeny in Gabon and the opening of the Francevillian intracratonic basins: A review: The 2-Ga Eburnean Orogeny in Gabon and the opening of the Francevillian intracratonic basins: A review. *Comptes Rendus Geoscience*, *348*(8), 572–586. https://doi.org/10.1016/j.crte.2016.07.003ï

Wiedenbeck, M., Allé, P., Corfu, F., Griffin, W. L., Roddick, J. C., & Speigel, W. (1995). Three natural zircon standards for U-Th-Pb, Lu-Hf, Trace element and REE analyses. *Geostandard Newsletter*, *19*(1), 1–23.

Zutterkirch, I. C., Kirkland, C. L., Barham, M., & Elders, C. (2021). Thin-section detrital zircon geochronology mitigates bias in provenance investigations. *Journal of the Geological Society, 179*(2). https://doi.org/10.6084/m9.figshare.c.5628911

Lihtlitsents lõputöö reprodutseerimiseks ja üldsusele kättesaadavaks tegemiseks

Mina, Carmel Kuusk,

1. annan Tartu Ülikoolile tasuta loa (lihtlitsentsi) minu loodud teose

***In situ* detrital zircon U-Pb age dating of Lastoursville Sub-Basin carbonate-black shale deposits in Francevillian Basin, Gabon,**

mille juhendaja on Kalle Kirsimäe,

reprodutseerimiseks eesmärgiga seda säilitada, sealhulgas lisada digitaalarhiivi DSpace kuni autoriõiguse kehtivuse lõppemiseni.

2. Annan Tartu Ülikoolile loa teha punktis 1 nimetatud teos üldsusele kättesaadavaks Tartu Ülikooli veebikeskkonna, sealhulgas digitaalarhiivi DSpace kaudu Creative Commonsi litsentsiga CC BY NC ND 4.0, mis lubab autorile viidates teost reprodutseerida, levitada ja üldsusele suunata ning keelab luua tuletatud teost ja kasutada teost ärieesmärgil, kuni autoriõiguse kehtivuse lõppemiseni.

3. Olen teadlik, et punktides 1 ja 2 nimetatud õigused jäävad alles ka autorile.

4. Kinnitan, et lihtlitsentsi andmisega ei riku ma teiste isikute intellektuaalomandi ega isikuandmete kaitse õigusaktidest tulenevaid õigusi.

Carmel Kuusk

24.05.2024